

The effect of neutron fluence on the
superconducting properties of Nb_3Sn

by

Chien Shih

A Thesis Submitted to the
Graduate Faculty in Partial Fulfillment of the
Requirements for the Degree of
MASTER OF SCIENCE

Major: Nuclear Engineering

Signatures have been redacted for privacy

Iowa State University
Ames, Iowa

1984

TABLE OF CONTENTS

	Page
I. INTRODUCTION	1
II. LITERATURE REVIEW	6
A. Transition Temperatures	6
B. Critical Currents and Fields	8
III. EXPERIMENTAL	13
A. Samples	13
B. Neutron Irradiation	13
C. Transition Temperature T_c Determination	15
D. Critical Current Density J_c Determination	20
E. Upper Critical Field H_{c2} Determination	20
IV. RESULTS	21
V. DISCUSSION	42
VI. SUMMARY AND CONCLUSIONS	55
VII. SUGGESTIONS FOR FURTHER STUDY	57
VIII. REFERENCES	58
IX. ACKNOWLEDGMENTS	60

LIST OF FIGURES

	Page
Figure 1. Neutron flux in different regions of a typical conceptual fusion reactor with a total wall loading of 10 MW/m^2 . (After McCracken and Blow, 1)	4
Figure 2. Critical current of Nb_3Sn multifilamentary wires as a function of applied magnetic field for a series of reactor neutron fluences. (After Snead, 17)	11
Figure 3. The dewar system	16
Figure 4. Circuit diagram of the mutual inductance comparison bridge	18
Figure 5. Transition temperature T_c as a function of high energy neutron fluence ($E > 1 \text{ MeV}$). The measurements of T_c were performed using resistance technique	22
Figure 6. Transition temperature T_c versus high energy neutron fluence. The measurements of T_c were performed using an ac susceptibility technique	23
Figure 7. Comparison of measurements of the reduced transition temperature (i.e. normalized to the unirradiated value, T_{c0}) as a function of high energy neutron fluence	24
Figure 8. The critical current density of $\text{Nb}_3\text{Sn-Cu}$ wires (30 wt % Nb, $R = 4600$) as a function of applied magnetic field for neutron fluence up to $1.3 \times 10^{19} \text{ n/cm}^2$ ($E > 1 \text{ MeV}$)	26
Figure 9. The critical current density of $\text{Nb}_3\text{Sn-Cu}$ wires (20 wt % Nb, $R = 30000$) as a function of applied magnetic field for neutron fluence up to $1.3 \times 10^{19} \text{ n/cm}^2$ ($E > 1 \text{ MeV}$)	27
Figure 10. The critical current density of $\text{Nb}_3\text{Sn-Cu}$ wires (30 wt % Nb, $R = 4600$) as a function of neutron fluence for several values of applied magnetic field	28

	Page
Figure 11. The critical current density of Nb ₃ Sn-Cu wires (20 wt % Nb, R = 30000) as a function of neutron fluence for several values of applied magnetic field	29
Figure 12. The critical current density of Nb ₃ Sn-Cu wires (20 wt % Nb, R = 2500) as a function of applied magnetic field for neutron fluence up to 1.3×10^{19} n/cm ² (E > 1 MeV)	30
Figure 13. The critical current density of Nb ₃ Sn-Cu wires (20 wt % Nb, R = 2500) as a function of neutron fluence for several values of applied magnetic field	31
Figure 14. The critical current density of Nb ₃ Sn-Cu wires (20 wt % Nb, R = 4600) as a function of applied magnetic field for neutron fluence up to 1.3×10^{19} n/cm ² (E > 1 MeV)	32
Figure 15. The critical current density of Nb ₃ Sn-Cu wires (20 wt % Nb, R = 4600) as a function of neutron fluence for several values of applied magnetic field	33
Figure 16. Reduced critical current density J_c/J_{c0} of Nb ₃ Sn-Cu wires (20 wt % Nb, R = 4600) plotted as a function of neutron fluence for several applied fields	35
Figure 17. Plot of $J_c^{1/2} B^{1/4}$ versus $\mu_0 H$ for Nb ₃ Sn-Cu wires (30 wt % Nb, R = 4600) after irradiation	37
Figure 18. Plot of $J_c^{1/2} B^{1/4}$ versus $\mu_0 H$ for Nb ₃ Sn-Cu wires (20 wt % Nb, R = 30000) after irradiation	38
Figure 19. Plot of $J_c^{1/2} B^{1/4}$ versus $\mu_0 H$ for Nb ₃ Sn-Cu wires (20 wt % Nb, R = 2500) after irradiation	39
Figure 20. Plot of $J_c^{1/2} B^{1/4}$ versus $\mu_0 H$ for Nb ₃ Sn-Cu wires (20 wt % Nb, R = 4600) after irradiation	40
Figure 21. Normalized critical current density as a function of transition temperature reduction ΔT_c for Nb ₃ Sn-Cu wires (30 wt % Nb, R = 4600) upon irradiation	45

	Page
Figure 22. Normalized critical current density as a function of transition temperature reduction ΔT_c for Nb ₃ Sn-Cu wires (20 wt % Nb, R = 4600) upon irradiation	46
Figure 23. Comparison of H_{c2} and T_c for Nb ₃ Sn-Cu wires (20 wt % Nb, R = 2500)	48
Figure 24. Critical current density of a family of Nb ₃ Sn-Cu <u>in situ</u> wires versus neutron fluence at 14 Tesla	49
Figure 25a. The critical current density as a function of applied magnetic field for neutron fluence up to 1.3×10^{19} n/cm ² (E > 1 MeV). The dashed line and the dot-dash line, model-1 calculations which assume that T_c is the only variable changed upon irradiation, are for 7.5×10^{18} n/cm ² and 1.3×10^{19} n/cm ² , respectively	52
Figure 25b. Comparison of the data with model-1 calculations which assume that T_c is the only variable changed, and with model-2 calculations which assume that T_c and ρ_N are the only variables changed upon irradiation. Dashed line (model-1) and dotted line (model-2) are for 7.5×10^{18} n/cm ² . Dot-dash line (model-1) and crossed line (model-2) are for 1.3×10^{19} n/cm ²	53

LIST OF TABLES

	Page
Table 1. The characteristics of Nb ₃ Sn-Cu samples	14
Table 2. Upper critical fields; H _{c2}	36

I. INTRODUCTION

Energy availability is of great concern to all nations. The production and distribution of food, transportation, employment, leisure activities, education, social and medical services, defense, in short nearly everything which contributes to a "good life" depends on energy. There is national and international uncertainty about future energy demands and about the sources which will provide the energy which will be actually consumed in the future. Prudent planning must take into account situations which approach the worst possible; thus, increases in demand must be assumed as must the retirement of traditional energy sources. Among the new sources, energy from nuclear fusion has a tremendous potential. This thesis deals with one important aspect of one type of fusion reactor.

Fusion is the name given to a class of nuclear reactions which involve the fusing of two or more light nuclei into a heavier nucleus with an associated energy release which, on a unit mass basis, is very large; larger than that provided by nuclear fission which, in turn, is very much larger than the energy provided by the combustion of coal, oil, or gas.

The fusion reaction is accomplished, in the magnetic confinement case, by confining the energetic reacting nuclei, which are in an ionic form, by magnetic means. The required magnetic fields are large both in magnitude and in volume. The I^2R heat loss in the magnet core windings is also large and, unless avoided, causes a significant reduction in the overall fusion system efficiency.

It has been generally agreed that the magnets needed to confine the high-energy plasma in fusion reactors will have to be superconducting. This implies that magnets for fusion reactor applications must satisfy exacting specifications over the lifetime of the system while being subjected to conditions which include factors unique to the fusion application as well as others which are relatively conventional. Among the conventional conditions are static and dynamic stresses, which may be asymmetric, associated with the changing magnetic field, and dependent on temperature changes including thermal cycling as the system alternates between operating and shut down conditions. The unique conditions include the radiation environment and the magnitude of the required field (7-14 Tesla). Ideally, the fusion reactor system should be able to operate essentially continuously for a normal 30 or 40-year power plant lifetime. Thus, the superconducting material used for the magnet coils must be evaluated with these various considerations in mind. A determination of the combined influence of all of these factors on the superconductor performance is far beyond the present state of material testing programs. However, the effects of some of these factors have received considerable attention during the past few years. The one discussed in this work is the influence of a radiation environment on the properties of candidate magnet components, particularly the effect on the superconducting transition temperature T_c , the critical current density J_c and the upper critical field H_{c2} .

The energy released from D-T fusion appears as the kinetic energies of alpha particles (3.5 MeV) and neutrons (14.1 MeV). Although the

neutrons are produced with energies of 14.1 MeV, when they reach the region occupied by the magnets, their energy distribution is predicted to be similar to that of fission neutrons (1). It is, therefore, possible to gain meaningful information concerning the behavior of superconducting materials to be used in fusion reactors by irradiation with neutrons from a fission reactor. The range of expected neutron fluences in the magnet region has been calculated by McCracken and Blow (1). As can be seen from Figure 1, the neutron flux at the location of the magnet coils depends primarily on the attenuation produced by the blanket/shield system and on the neutron first wall loading. McCracken and Blow showed that the neutron flux incident on the first wall will be attenuated by a factor of about 1.6×10^{-6} in reaching the magnet region. As shown in Figure 1, this is achieved by a blanket and shield thickness of 100 and 55 cm, respectively. For a total first wall loading of 10 MW/m^2 , the neutron flux ($E > 0.1 \text{ MeV}$) will be around $4 \times 10^9 \text{ n/cm}^2 \cdot \text{sec}$ at the inside edge of the winding. After ten years of continuous fusion reactor operation at this flux level, the fluence ($\int \phi dt$) would be $1.2 \times 10^{18} \text{ n/cm}^2$ ($E > 0.1 \text{ MeV}$). These values may be compared with the much lower values developed for the UWMAK-II reactor concept: wall loading = 1.16 MW/m^2 and attenuation factor of about 6×10^{-8} . However, because the shielding may be difficult to construct or install and thus, will be less effective at certain locations, "hot-spots" may develop. Thus, the effect of irradiation on superconductors should be determined for doses at least a factor of 10 larger than the predicted lifetime dose. As shown by these examples, a neutron fluence of $2.0 \times 10^{18} \text{ n/cm}^2$

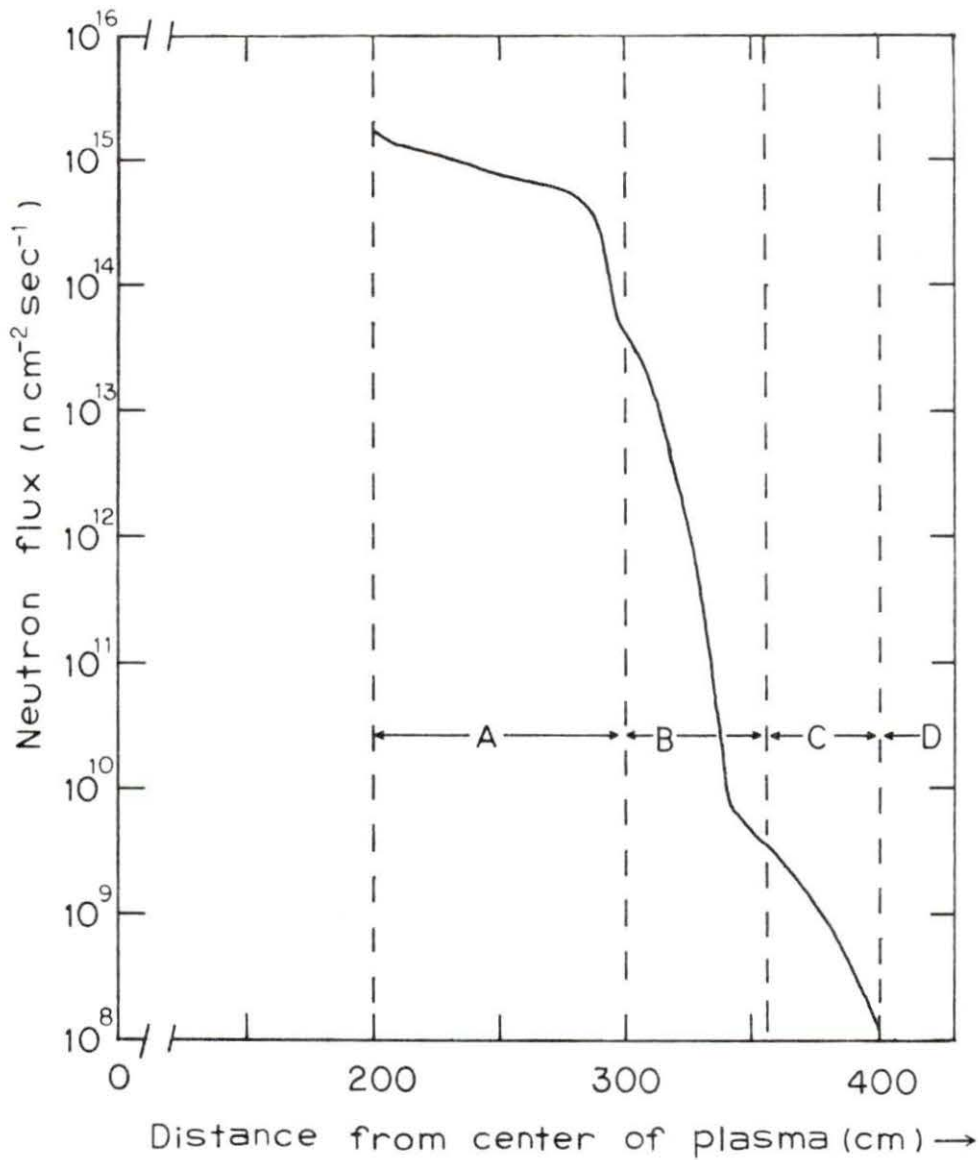


Figure 1. Neutron flux in different regions of a typical conceptual fusion reactor with a total wall loading of 10 MW/m². (After McCracken and Blow, 1)

- A region: first wall, blanket, moderator, etc.
- B region: magnet shield.
- C region: magnet.
- D region: biological shield

($E > 1$ MeV) seems to be a reasonable estimate for a 10-year "lifetime" dose for the superconducting magnet.

The samples used for this study were prepared by the in situ process. In situ formed Nb_3Sn -Cu superconducting wire is made by casting a Nb-Cu melt to form a random array of Nb dendrites in a Cu matrix and drawing to wire. Tin is deposited on the wire and heat-treated to produce aligned Nb_3Sn filaments in a bronze matrix. The details of these techniques are described elsewhere (2). In situ superconducting composites have high critical current densities and good strain tolerances which make them attractive as potential magnet materials for Controlled Thermonuclear Reactor (CTR) applications. Their performance characteristics (2) all compare favorably with bronze-process material (3a). The major difference between in situ and bronze process material is that the superconducting filaments in the former are discontinuous and have much smaller dimensions. This morphology might possibly alter the susceptibility of these materials to degradation in an irradiation environment, so a series of experiments was carried out to determine these effects. In this study, the effect of high-energy neutron ($E > 1$ MeV) irradiation at ambient reactor temperature on the superconducting properties (T_c , J_c , H_{c2}) of in situ wires is reported. The most suitable potential superconducting magnet material for a future fusion reactor is selected from among the in situ wires studied.

This study is part of an ongoing research program on superconducting materials. The samples for this study were selected on the basis of the findings of Sue et al. (2). Arrangements for the neutron irradiation

of the samples were made by Finnemore through Dr. Snead of Brookhaven National Laboratory. To reach higher magnetic fluxes than can be achieved at ISU, the I_c measurements were carried out by Finnemore and Ostenson at Francis Bitter Magnet Laboratory at MIT. A preliminary report on some of the results was given by Finnemore at an IEEE meeting (3b). T_c measurements using resistivity and ac susceptibility techniques were carried out at ISU by Shih and Ostenson. The I_c and T_c data collected by Finnemore, Ostenson, and Shih were analyzed, plotted, and discussed by Shih and form part of this thesis.

II. LITERATURE REVIEW

A few A-15 superconducting compounds have been favored for practical applications because they show high transition temperature, high critical current and high critical field. In contrast with these desirable features, it has been reported that these compounds are sensitive to radiation, that is, their superconducting properties are seriously degraded by radiation. In the following paragraphs, the effects of irradiation on the transition temperature T_c , the critical current density J_c (or critical current I_c), and the upper critical field H_{c2} of Nb_3Sn are reviewed.

A. Transition Temperatures

Swartz et al. (4) irradiated Nb-based A-15 powdered compounds with high energy neutrons at ambient reactor temperature to a fluence of about 1.5×10^{18} n/cm². T_c was found to decrease by 0.10 K and 0.08 K for arc-cast Nb_3Sn and diffusion-processed Nb_3Sn , respectively. Very little change in the transition temperature was observed by Cooper (5) as the result of neutron irradiation of vapor-deposited Nb_3Sn samples. For a sample of Nb_3Sn deposited on ceramic plate with an unirradiated T_c of 18.33 K, no change in magnitude of the transition temperature was observed after exposure to a fluence of 4.7×10^{17} n/cm². After an exposure of 2.7×10^{18} n/cm², the transition temperature decreased by 0.18 ± 0.02 K. Bett (6) irradiated Nb_3Sn tapes to higher fluences ($\sim 5 \times 10^{19}$ n/cm²) than previous workers, and observed very large reductions in T_c ($\Delta T_c = 13$ K). He also noted that T_c could be restored

to the unirradiated value by annealing at 900°C for two hours. Following Bett's work, Sweedler et al. (7) irradiated various Nb-based A-15 compounds to fluence levels of 5×10^{19} n/cm² ($E > 1$ MeV) and found that large reductions, ($\Delta T_c \leq 17$ K), in T_c were observed for Nb₃Sn. They also showed that recovery to the unirradiated value of T_c for Nb₃Sn could be accomplished by annealing at 750°C for 20.5 hours. They assumed that the interchange of atoms between sites, which is the principal result of neutron irradiation, was the reason for this large, reversible change in the superconducting transition temperature T_c of Nb₃Sn. Bauer et al. (8) also observed large T_c depressions for the A-15 compound Nb₃Sn when doped with U²³⁵ and B¹⁰ and irradiated with thermal neutrons. Irradiations with fast neutrons ($E > 1$ MeV) were also carried out: a T_c decrease by 6.4 K was observed for Nb₃Sn.

Most reports deal with the effect of neutron irradiation at high temperatures (e.g., ambient reactor temperatures, 60°C - 140°C). Soell et al. (9) performed an experiment on Nb₃Sn diffusion wires to measure the T_c reduction after neutron irradiation at low temperature. They observed a decrease in T_c of about 0.8 K following an irradiation at 4.6 K to a fluence of 3.9×10^{18} n/cm² ($E > 0.1$ MeV). Later, Soell et al. (10) irradiated Nb₃Sn diffusion wires to higher fluences at higher temperature ($T = 10$ K). The value of T_c remained essentially constant until the fast neutron fluence ($E > 0.1$ MeV) exceeded 10^{18} n/cm². T_c , then, decreased linearly to about 14.2 K (i.e. $\Delta T_c = 3.8$ K) as the neutron fluence was increased to a maximum of 1.05×10^{19} n/cm².

B. Critical Currents and Fields

Cullen and Novak (11) and Cullen et al. (12) irradiated vapor-deposited Nb₃Sn strips with high energy neutrons at 50°C to fluences of less than 10¹⁸ n/cm², and observed increases in I_c that were for the most part independent of applied transverse field up to 20 KG (1 Tesla = 10 KG). These increases were attributed to increased pinning of the defects formed by the irradiation. Later, Cullen and Novak (13), working with vapor-deposited Nb₃Sn strips, reported irradiation induced increases in I_c for samples with low J_{c0} (the J_c prior to irradiation), but decreases in I_c for samples with higher J_{c0}. Soell et al. (9) found that reactor neutron irradiation to 3.9 x 10¹⁸ n/cm² (E > 0.1 MeV) at 4.6 K produced an increase in I_c in Nb₃Sn wires made by vapor-phase diffusion. There was partial recovery of I_c upon annealing at 250 K for 10 minutes, but a small further decrease in T_c was noted during these anneals. These observations can be explained by assuming that the larger interstitial or vacancy clusters, which are produced during annealing after irradiation, have a strong influence on the transition temperature T_c.

After the development of a solid-state diffusion "bronze-processed" Nb₃Sn (which provided a high critical current density), radiation effects, on what appears to be engineering-grade material, could be determined. Although some of the investigators, whose results were noted above, observed small decreases in both T_c and I_c following initial increases in I_c at relatively low fluences, large decreases in critical properties below preirradiation values were not observed until the high-fluence

work of Parkin and Schweitzer (14) was reported. They irradiated multifilamentary Nb₃Sn wires with fast neutrons to fluences of 6×10^{19} n/cm² ($E > 1$ MeV) at 60°C. They observed that the critical current drops precipitously toward zero for neutron fluences somewhat greater than 10^{18} n/cm². Studies of the variation of T_c and I_c over the same fluence range led to the conclusion that reductions in I_c were caused by decreases in T_c . At a fluence of 6×10^{19} n/cm², the upper critical field of Nb₃Sn is reduced from the no fluence value of 240 KG to 9 ± 0.5 KG. A decrease in I_c as a function of applied transverse magnetic field at 4.2 K was observed for fields of up to 40 KG and for fluences up to 6×10^{19} n/cm². Brown et al. (15) investigated this low-field (< 40 KG) and low-fluence ($\leq 2 \times 10^{18}$ n/cm²) regime in some detail. They observed that J_c could be increased upon irradiation with fast neutrons at 6 K. The increase is largest at their highest applied field (~ 30 KG), with decreases occurring at low fields (< 15 KG). As the dose is increased, J_c increases to a saturation value and then decreases for higher doses. The saturation dose is largest for the highest field. This J_c enhancement, therefore, is very field dependent. Brown et al. interpreted the rise in J_c as due to increased flux pinning by radiation-induced cascades and the subsequent decrease of J_c at high fluence as due to a saturation in the cascade pinning that occurs above the dose at which the deleterious effects of the T_c and H_{c2} changes become significant. For Nb₃Sn wires, no changes in J_c similar to those described above were observed by Parkin and Sweedler (16) for reactor neutron irradiation doses $< 2 \times 10^{18}$ n/cm² ($E > 1$ MeV) at 60°C. These

doses fall within the regime where substantial increases in J_c were observed by Brown et al. (15); however, the temperature at which the irradiation took place was 6 K. The large decreases in J_c for higher doses are attributed to decreases in T_c . Therefore, although the radiation-induced disorder and resultant T_c decreases are comparable for 6 K and 60°C irradiation, the different type of radiation-induced structure have substantially different effects on the flux pinning. From the results on Nb, Brown concluded that, at low doses, the defect cascades present for 6 K irradiation are much more effective for flux pinning than are the clusters or loops present after irradiations of equal dose at 60°C. This is also true for Nb₃Sn.

Snead (17) reported, as shown in Figure 2, the effect of neutron irradiation on the I_c of multifilamentary Nb₃Sn wires for neutron fluences from 6×10^{17} n/cm² to 3.6×10^{19} n/cm² ($E > 1.0$ MeV) as a function of applied transverse magnetic field up to 160 KG (16 Tesla). The values of H_{c2} for various neutron fluences were obtained by extrapolating the high-field part of the curve to the H axis for a value of critical current of 0.01 A. For applied magnetic field $H > 40$ KG, he defined two regions of change in I_c upon irradiation. First, I_c increased with increasing fluence up to a maximum at 1.0×10^{18} n/cm². Values of H_{c2} were greater than those observed for the unirradiated cases with the maximum value occurring for a dose of 1.0×10^{18} n/cm² corresponding to the largest increase in I_c . In the second region, both I_c and H_{c2} decreased rapidly for doses above 1.0×10^{18} n/cm². The Hake's expression (18a) for the upper critical field was used by him to

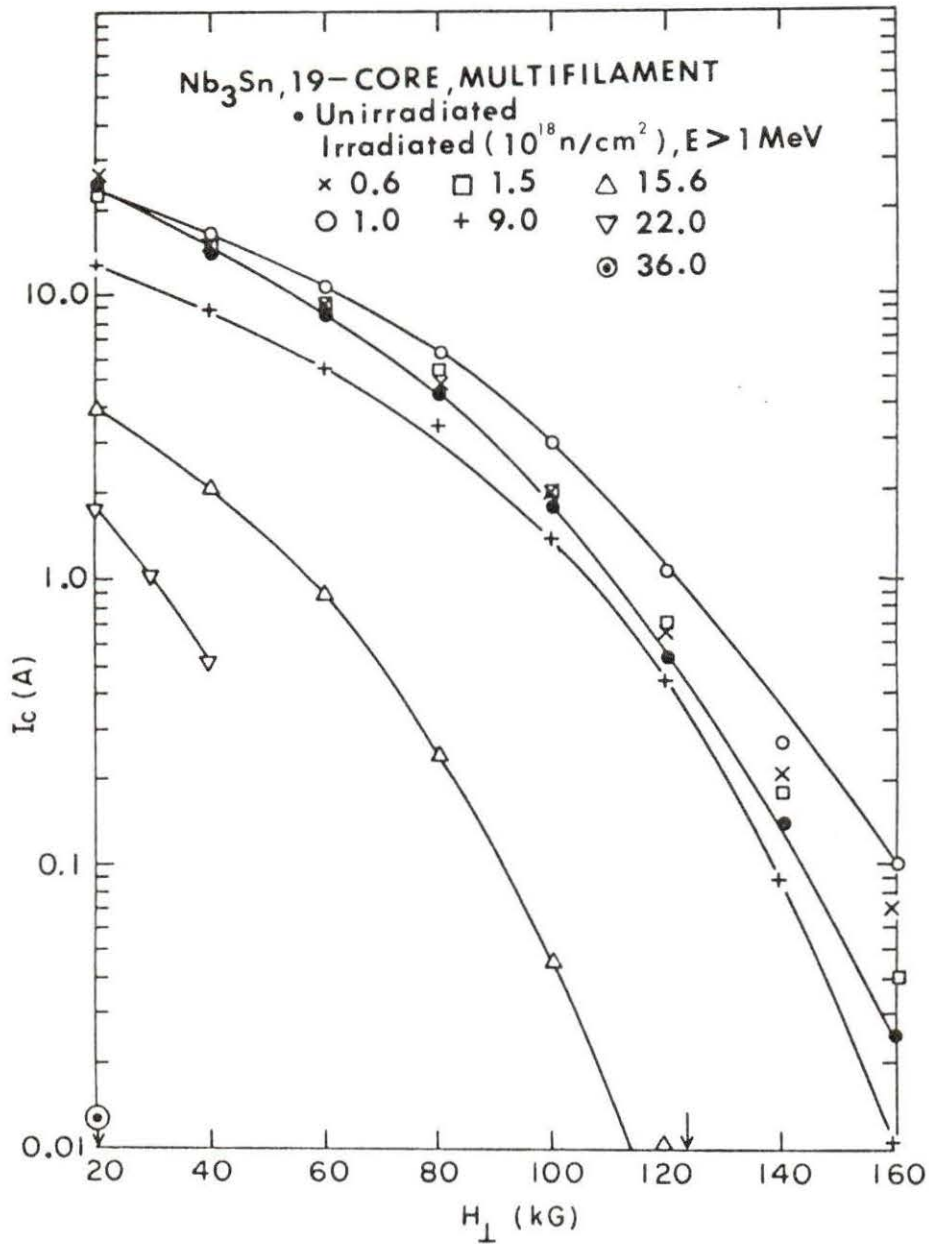


Figure 2. Critical current of Nb₃Sn multifilamentary wires as a function of applied magnetic field for a series of reactor neutron fluences. (After Snead, 17)

explain these changes. The expression can be written in the form

$$H_{c2} = 3.06 \times 10^4 \gamma T_c \rho_N$$

where γ = electronic specific-heat coefficient,

T_c = usual transition temperature, and

ρ_N = normal-state resistivity of the superconductor.

The damage induced by the neutron irradiation increases ρ_N . He also observed that T_c does not change significantly over the first fluence range (i.e. below 1.0×10^{18} n/cm²), and γ is not expected to be affected by the neutron irradiation. Thus, in the fluence range below 1.0×10^{18} n/cm², the increases observed in I_c due to an increasing H_{c2} are attributed to increases of ρ_N caused by the irradiation. Within the second fluence range (i.e. above 1.0×10^{18} n/cm²), the decreasing characteristic of T_c dominates in the above expression for the upper critical field, thereby causing the large decreases in I_c for increasing fluence.

III. EXPERIMENTAL

A. Samples

Nb_3Sn -Cu samples fabricated by the in situ process were supplied by Dr. J. D. Verhoeven and Dr. D. K. Finnemore of the Ames Laboratory of the DOE. The detailed process of fabrication is described elsewhere (2). On the basis of the experimental results obtained by Sue et al. (2), four samples (i.e. composition and area reduction R) were selected for study. These samples yielded high values for J_c prior to neutron irradiation (2). The characteristics of these samples are presented in Table 1. The Cu-30 wt % Nb - 14.8 vol % Sn (R = 4600) sample provided the highest J_c . The sample yielding the second highest value of J_c depends on the strength of the applied magnetic field. For fields greater than 12 Tesla, it is the Cu-20 wt % Nb - 9.3 vol % Sn (R = 2500) sample, whereas for fields less than 12 Tesla, it is the Cu-20 wt % Nb - 9.3 vol % Sn (R = 4600) sample. The fourth sample, Cu-20 wt % Nb - 9.3 vol % Sn (R = 30000), yields a value for J_c which is somewhat lower than that for the other three samples. This reduction in J_c is due to the effect of severe coarsening accompanying the area reduction.

B. Neutron Irradiation

The neutron irradiations were carried out in the Brookhaven High Flux Beam Reactor (HFBR). The wire specimens were sealed in 4-mm quartz tubes containing 0.5 atm of helium gas. The quartz tubes were placed in aluminum irradiation capsules filled with H_2O to facilitate heat transfer. The temperature of the specimens during irradiation was

Table 1. The characteristics of Nb₃Sn-Cu samples

Designation	Sample	Heat treatment	Area reduction ratio R ^a	Final diameter cm
1	Cu-30 wt % Nb - 14.8 vol % Sn	550°C 5 days	4600	0.016
2	Cu-20 wt % Nb - 9.3 vol % Sn	550°C 5 days	2500	0.015
3	Cu-20 wt % Nb - 9.3 vol % Sn	550°C 5 days	4600	0.015
4	Cu-20 wt % Nb - 9.3 vol % Sn	550°C 5 days	30000	0.015

^aArea reduction ratio R is defined as A_i/A_f , where A_i is the initial sample area before mechanical reduction and A_f is the final area.

estimated to be $\sim 80^{\circ}\text{C}$. The irradiating neutron flux was 1.3×10^{14} $\text{n/cm}^2 \cdot \text{sec}$ for neutron energies $E > 1$ MeV. The flux of neutrons with energy $E > 0.11$ MeV was 5.64×10^{14} $\text{n/cm}^2 \cdot \text{sec}$. In this study, the effects of neutron fluences of 3.0×10^{17} n/cm^2 , 6.5×10^{17} n/cm^2 , 2.5×10^{18} n/cm^2 , 7.5×10^{18} n/cm^2 , and 1.3×10^{19} n/cm^2 are presented.

C. Transition Temperature T_c Determination

Variations in temperature of the superconducting material within a relatively narrow range are accompanied by large changes in such parameters as the resistivity and ac susceptibility. The transition temperature is defined as being the temperature midway between the 10% and 90% of the superconducting-to-normal transition change however measured. The value of T_c is found by exploring the effect of temperature variation on appropriate parameters.

Measurements of T_c were carried out in the Physics Department laboratories at Iowa State University. The dewar system used to hold or vary the temperature, as required in this experiment, is shown in Figure 3. The liquid nitrogen dewar, liquid helium dewar and heat leak can were made of stainless steel.

The temperature range of interest in this experiment is above 4.2 K. Temperature control in the sample region was accomplished in the following manner. The heat leak chamber vacuum space was evacuated to a pressure of less than 10^{-3} Torr and the sample chamber was sealed at a pressure of less than 0.2 Torr. This pressure was chosen for the sample chamber since higher pressures permit convection currents with consequent heat loss and substantially lower pressures gave rise to

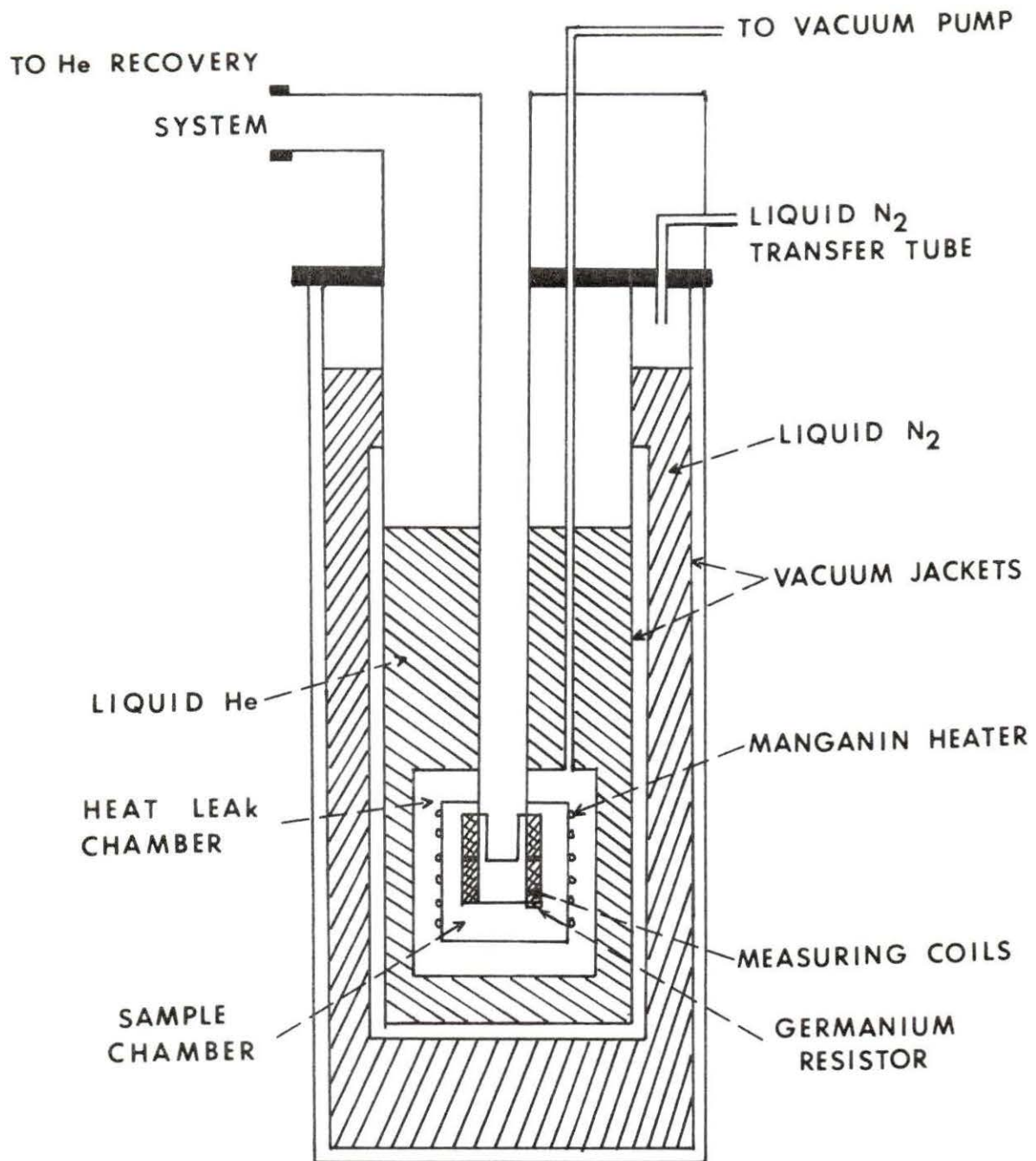


Figure 3. The dewar system

poor thermal equilibrium. Once the temperature stabilized below the desired value (e.g., 5 K), the manganin heater, astatically wound around the outside of the sample chamber, was used to elevate the temperature. The "superconducting-to-normal" transition can, therefore, be accomplished.

Measurements of T_c were made with both a standard 4 probe resistance technique and an ac susceptibility technique. A germanium resistor (GR 10086) was used as the thermometer for both measurements. The temperature dependent resistance of the germanium was obtained by measuring the voltage drop across the germanium resistor, when current through it was 10 μ a.

For T_c measurements made using the 4 probe resistance technique, the superconducting-to-normal transition curve was plotted on a Honeywell 550 X-Y recorder. The voltage across the germanium resistor (i.e. the "temperature") provided the X-signal. The potential drop across the superconducting sample, produced by a 1 ma current, was amplified by means of a Keithley 148 Nanovoltmeter and fed to the recorder as the Y-signal.

In order to obtain T_c by the ac susceptibility method, samples were placed in the center of measuring coils. A fixed frequency oscillator supplied a 100 Hz signal, which is required by a dual phase lock-in detector, to the primary coil which induced a voltage in the secondary coil. Variations in the voltage induced in the secondary coil due to transitions from the normal to the superconducting state were measured using a mutual inductance comparison bridge (Figure 4). The output

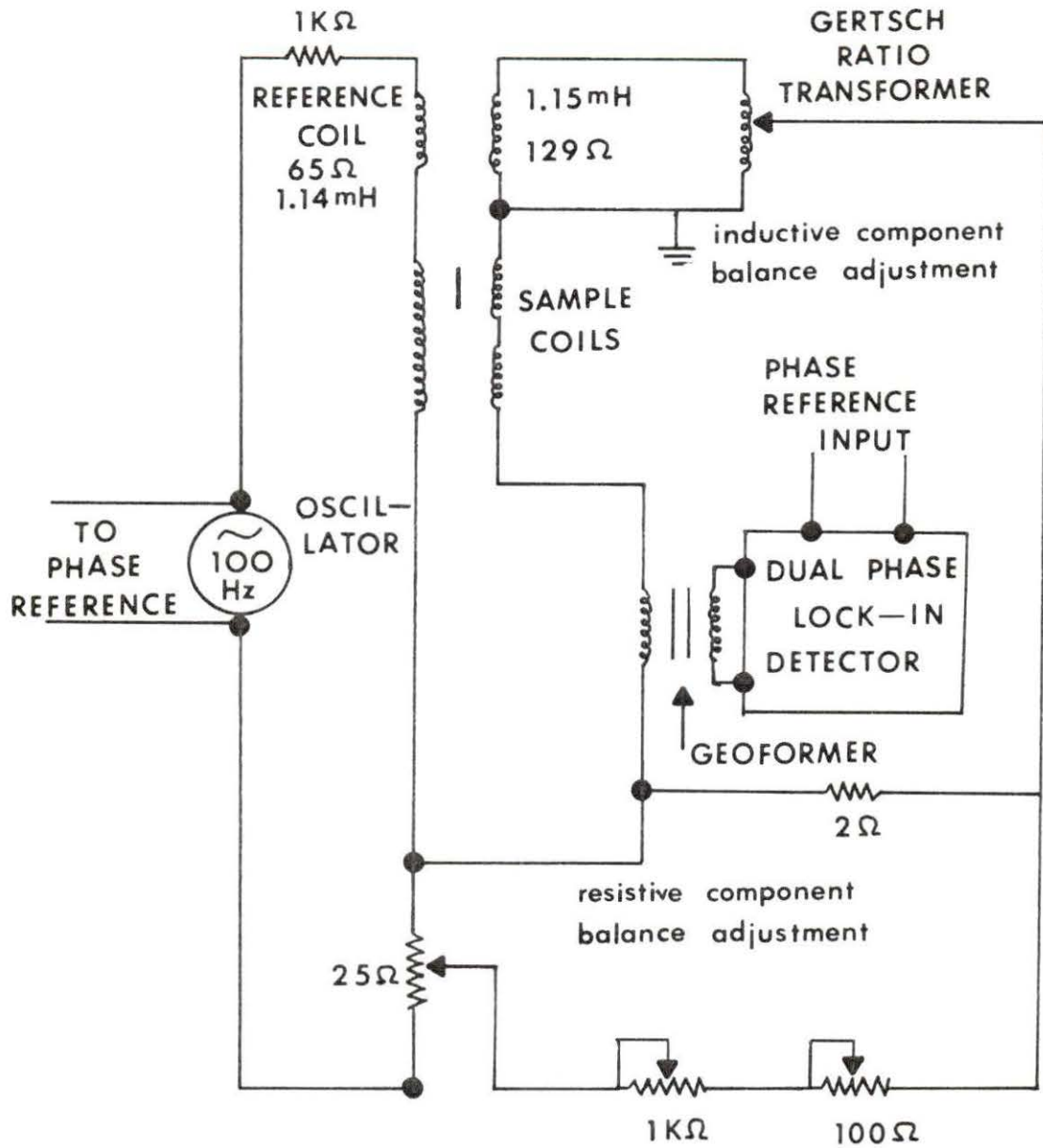


Figure 4. Circuit diagram of the mutual inductance comparison bridge

voltage has inductive and resistive components, the resistive component being due to eddy currents in the bridge network and the metal parts of the apparatus. In order to balance the bridge, both the inductive and resistive components must be separately balanced. The resistive voltage from the secondaries is balanced by the voltage across a 2Ω resistor placed in the detection portion of the bridge which is driven by a resistive network directly from the primary loop on the oscillator. The voltage introduced into the detection circuit is proportional to $1/(1100-R)$, where R is the setting of the variable resistors. The inductive component of the voltage from the secondaries is balanced by a voltage generated across a fixed reference coil. The inductive balancing voltage introduced into the detection circuit is proportional to the setting on the Gertsch Ratio Transformer which divides the output of the fixed reference coil.

A fixed frequency phase sensitive lock-in detector, locally built, was coupled to the circuit through a geoformer (i.e. a type of input transformer). A convenient feature of this detector is that both phases of an off balance signal are displayed on twin output meters. When the detector was properly phased, changes in inductive and resistive voltages of the susceptibility were independent of each other as long as the meters were on scale. The changes of inductive voltage during normal to superconducting transition were recorded on the Honeywell 550 X-Y recorder as the Y-signal, and the voltage drop across the germanium resistor provided the X-direction signal proportional to the temperature.

For superconducting transitions, 10% - 90% transition widths were used to denote the T_c ranges and the temperature at the midpoint of a transition was reported as transition temperature T_c . The accuracy of the transition temperature was within ± 0.01 K over the temperature range 4 - 20 K.

D. Critical Current Density J_c Determination

Critical current measurements were made in the magnetic field provided by a "Bitter type" solenoid at the National Magnet Laboratory of M.I.T. by Dr. D. K. Finnemore and J. E. Ostenson (18b). These measurements were obtained at 4.2 K (liquid He temperature) as a function of an applied transverse field of up to 15 Tesla. It is the convention to define the critical current as the current which produces a 1 μ V drop across a 1 cm length of the sample. In this work, critical current density was obtained by dividing the critical current by the total cross-section area of the sample.

E. Upper Critical Field H_{c2} Determination

The H_{c2} data were determined from a linear extrapolation of the plot of $J_c^{1/2} B^{1/4}$ versus $\mu_0 H$ to $J_c^{1/2} B^{1/4} = 0$.

IV. RESULTS

The change of the transition temperature, T_c , with neutron irradiation for a family of Nb_3Sn -Cu superconducting composites is shown in Figures 5 and 6. These results were obtained using resistance and ac susceptibility techniques, respectively. As shown in these figures, there is essentially no degradation of transition temperature for neutron fluences below 1×10^{18} n/cm². Above this fluence, a gradual decline in T_c begins and, for a fluence of 1.3×10^{19} n/cm², decreases of $\sim 9K$ and $\sim 8K$ were observed and are shown in Figures 5 and 6, respectively. For Nb_3Sn -Cu in situ wires with higher initial transition temperatures, such as 30 wt % Nb - 14.8 vol % Sn ($R = 4600$), the percent depression upon irradiation is almost the same as that found for lower-initial-transition-temperature wires. For comparison, the results obtained by Snead et al. (19) and Sweedler et al. (20), together with the data in Figures 5 and 6, are plotted in Figure 7. Here, T_c is normalized by its unirradiated value T_{c0} . The results found by Snead et al. for bronze-processed Nb_3Sn single core filamentary wires and Sweedler et al. for bulk Nb_3Sn are very similar to the present results for in situ wires. However, the leveling off, or saturation, shown by Sweedler's work, was not observed in this study since it occurs at fluences above those used in this work.

Results of the 4.2 K measurements of critical current density, J_c , for a family of Nb_3Sn -Cu wires as a function of applied transverse magnetic field and for neutron fluences up to 1.3×10^{19} n/cm² are presented in Figures 8, 9, 12 and 14. Examination of these figures

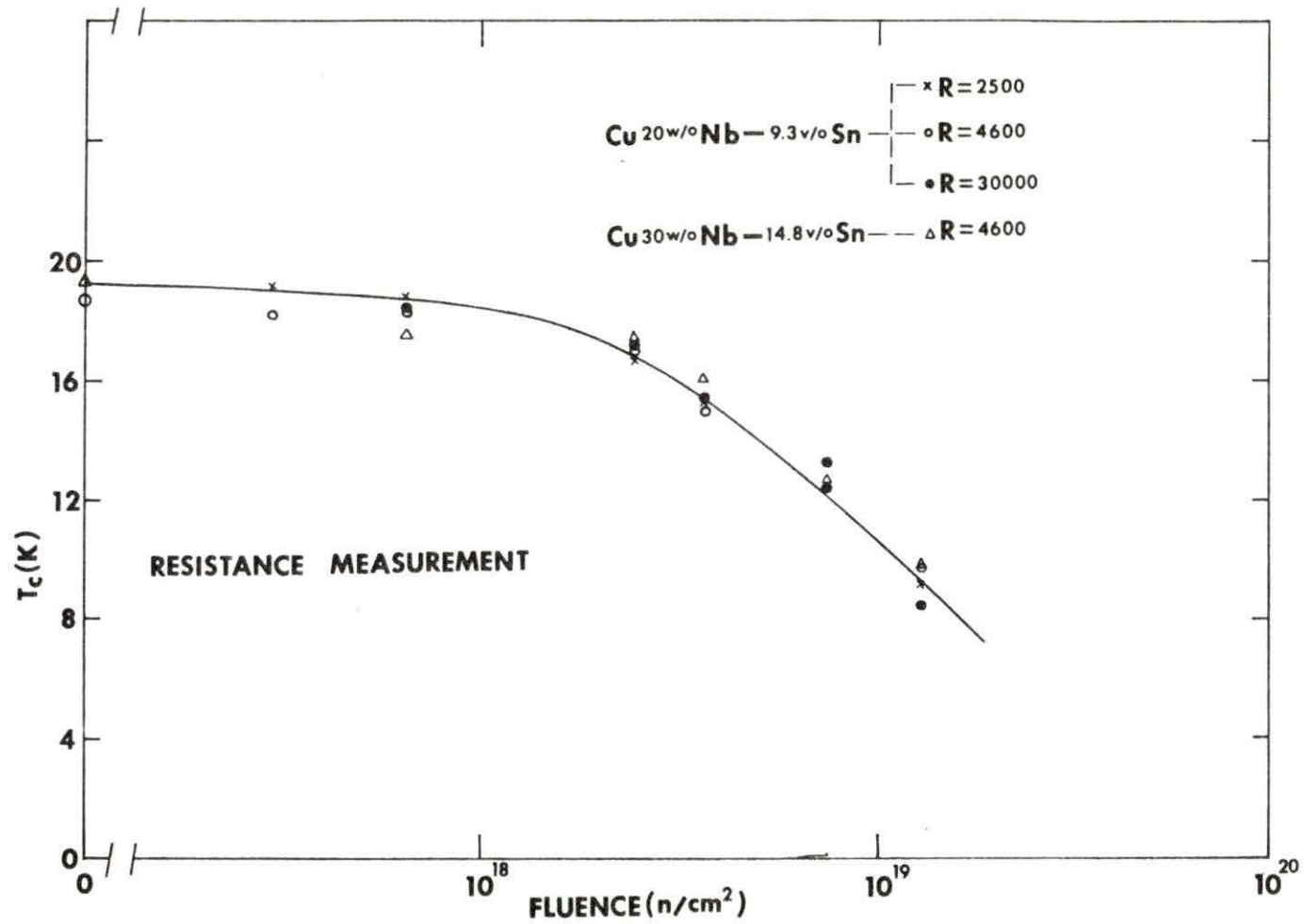


Figure 5. Transition temperature T_c as a function of high energy neutron fluence ($E > 1$ MeV). The measurements of T_c were performed using a resistance technique. (Solid line is for guiding the eye)

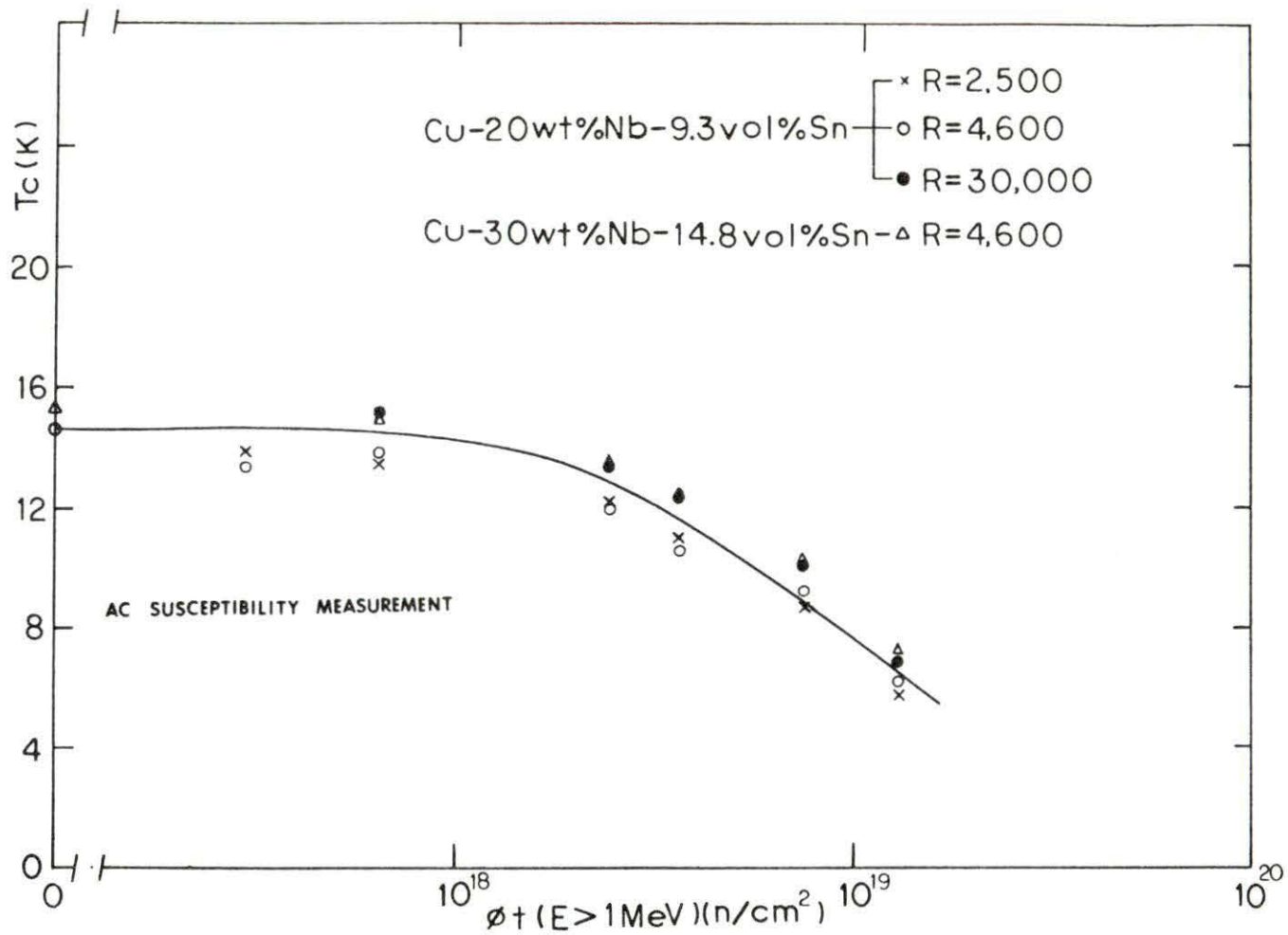


Figure 6. Transition temperature T_c versus high energy neutron fluence. The measurements of T_c were performed using an ac susceptibility technique. (Solid line is for guiding the eye)

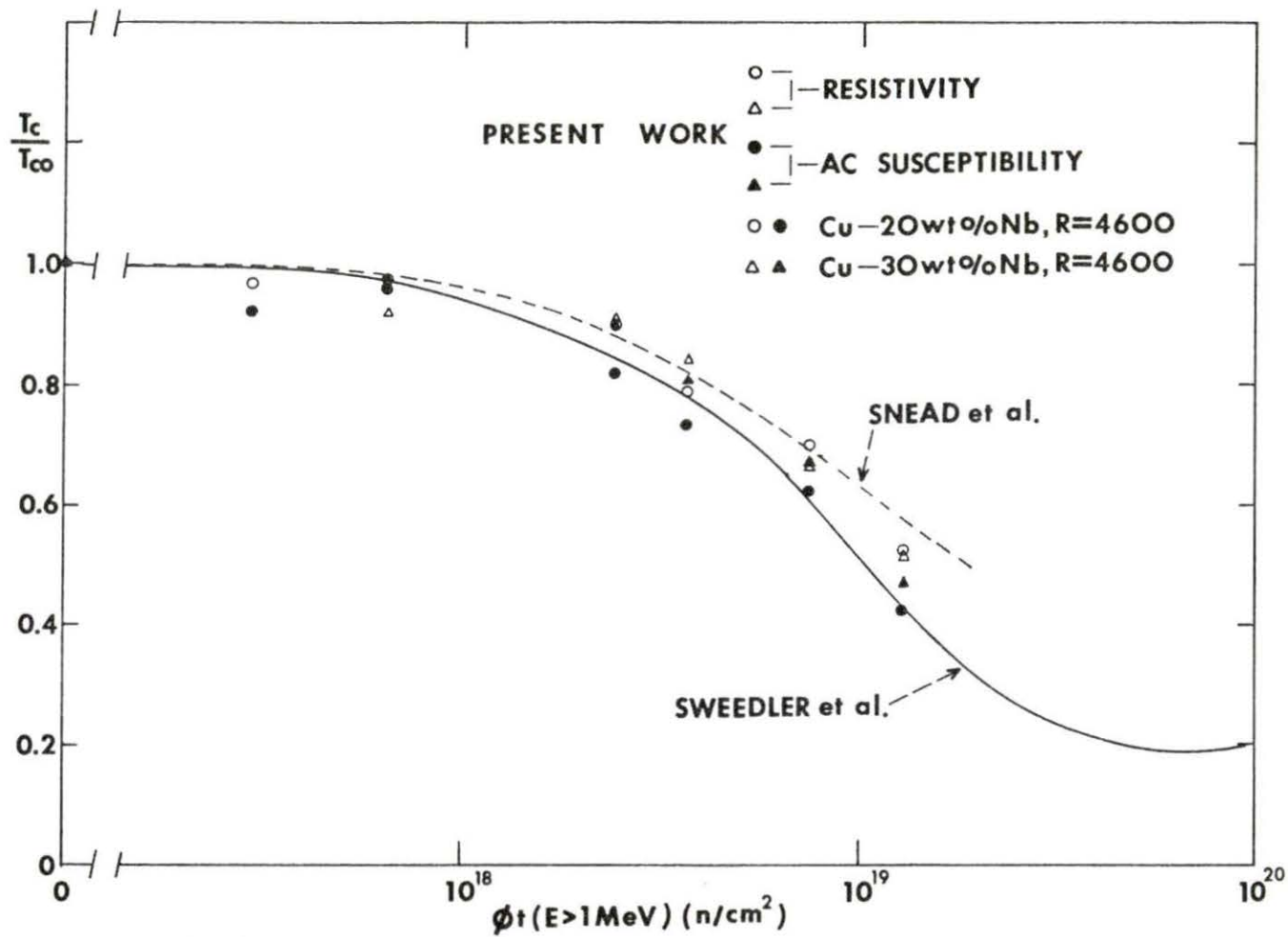


Figure 7. Comparison of measurements of the reduced transition temperature (i.e. normalized to the unirradiated value, T_{co}) as a function of high energy neutron fluence

reveals that there are three anomalous curves, the 6.5×10^{17} n/cm² curve on Figure 8, and the "unirradiated" and 2.5×10^{18} n/cm² curves on Figure 14. All three curves seem to have values of J_c which are too low for values of $\mu_0 H < 14$ T. Experience indicates that results of this kind can be obtained if the sample does not adhere properly to the backing surface. For 30 wt % Nb - 14.8 vol % Sn (R = 4600) (Figure 8) and 20 wt % Nb - 9.3 vol % Sn (R = 30000) (Figure 9) wires, J_c is seen to increase with fluence, pass through a maximum at 2.5×10^{18} n/cm², and then decrease. This behavior is shown clearly in Figures 10 and 11 where J_c is plotted versus fluence for several values of applied field. J_c increases with fluences and exhibits a broad peak centered at 2.5×10^{18} n/cm². In the region above 2.5×10^{18} n/cm², all curves in each figure drop off in the same precipitous fashion to smaller J_c at $\sim 1.3 \times 10^{19}$ n/cm².

The change in J_c upon irradiation for 20 wt % Nb - 9.3 vol % Sn (R = 2500) wires is shown in Figure 12. The critical current density increases with fluence up to 6.5×10^{17} n/cm² and then decreases with fluence. This behavior is also seen in Figure 13 where J_c is plotted versus fluence for several applied magnetic fields.

For 20 wt % Nb - 9.3 vol % Sn (R = 4600) wires, a behavior which differs from that of the other samples is observed. As shown in Figures 14 and 15, J_c increases as the fluence increases to 6.5×10^{17} n/cm² for applied magnetic fields up to 12 Tesla. For higher fluences, J_c decreases. Above 12 Tesla, the reduction of J_c begins for a fluence of 3.0×10^{17} n/cm². To show this behavior more clearly, the reduced

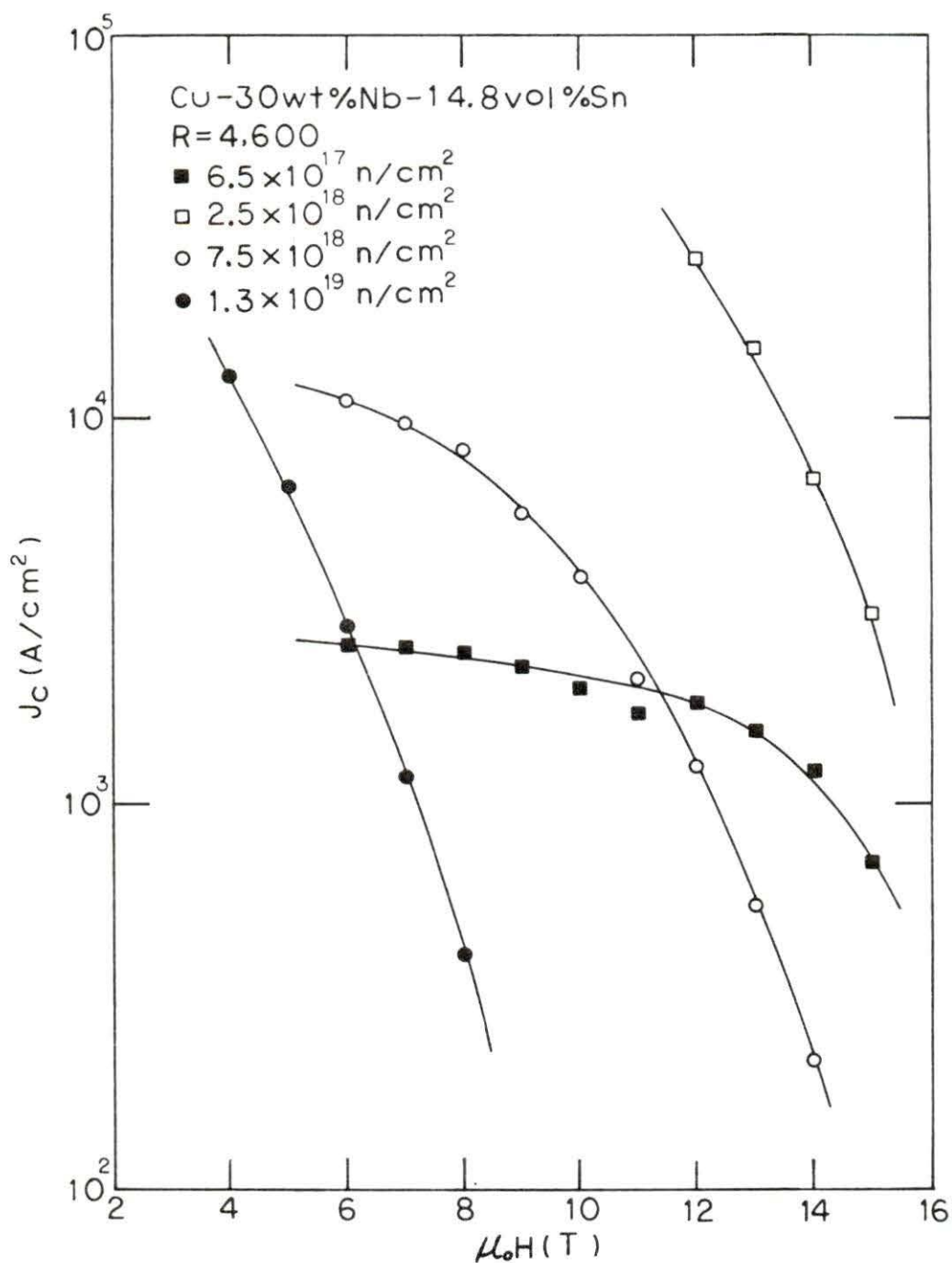


Figure 8. The critical current density of Nb₃Sn-Cu wires (30 wt % Nb, R = 4600) as a function of applied magnetic field for neutron fluence up to 1.3×10^{19} n/cm² ($E > 1$ MeV). (Data obtained by Finnemore et al.)

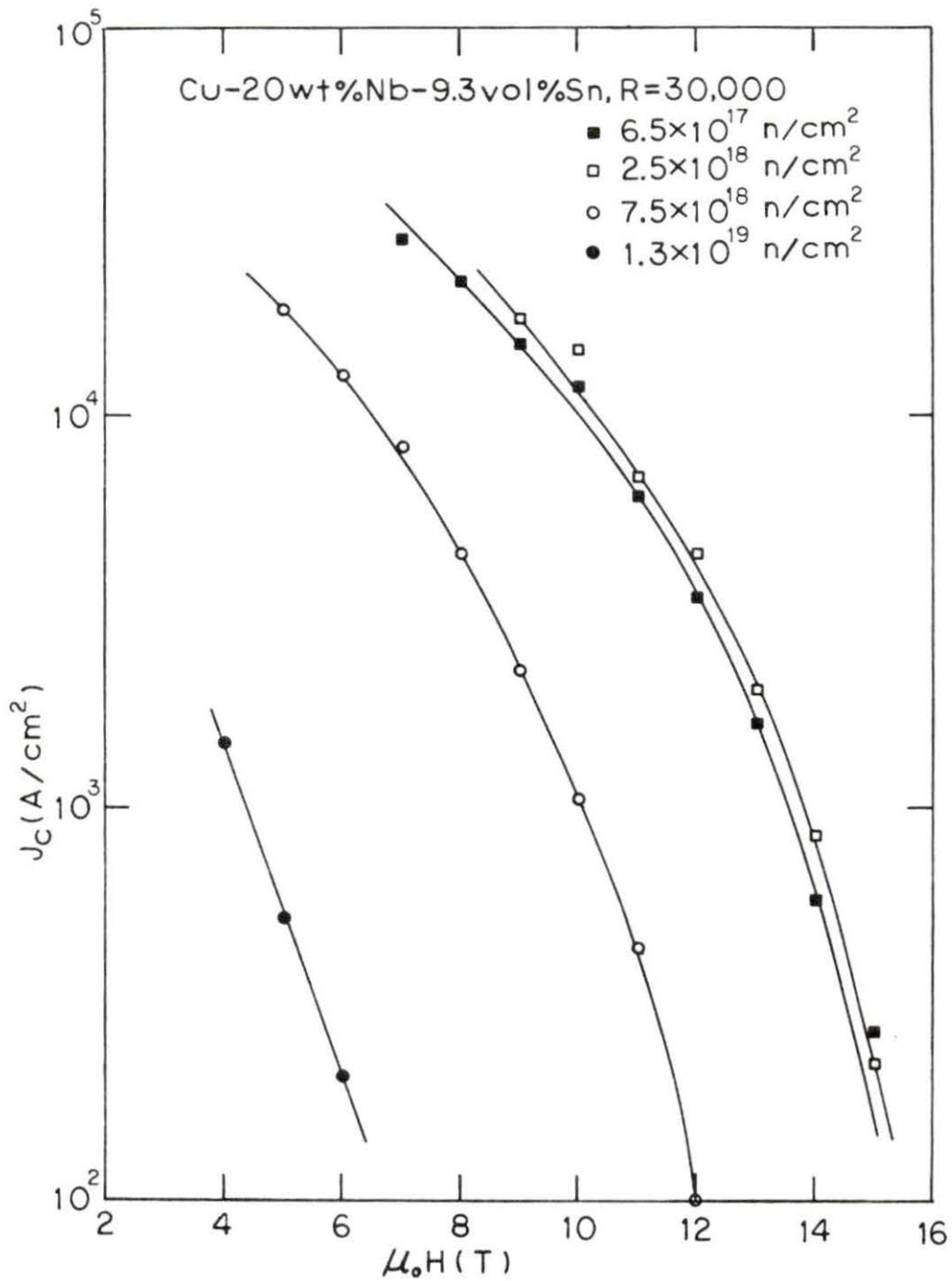


Figure 9. The critical current density of Nb₃Sn-Cu wires (20 wt % Nb, R = 30000) as a function of applied magnetic field for neutron fluence up to 1.3×10^{19} n/cm² ($E > 1$ MeV). (Data obtained by Finnemore et al.)

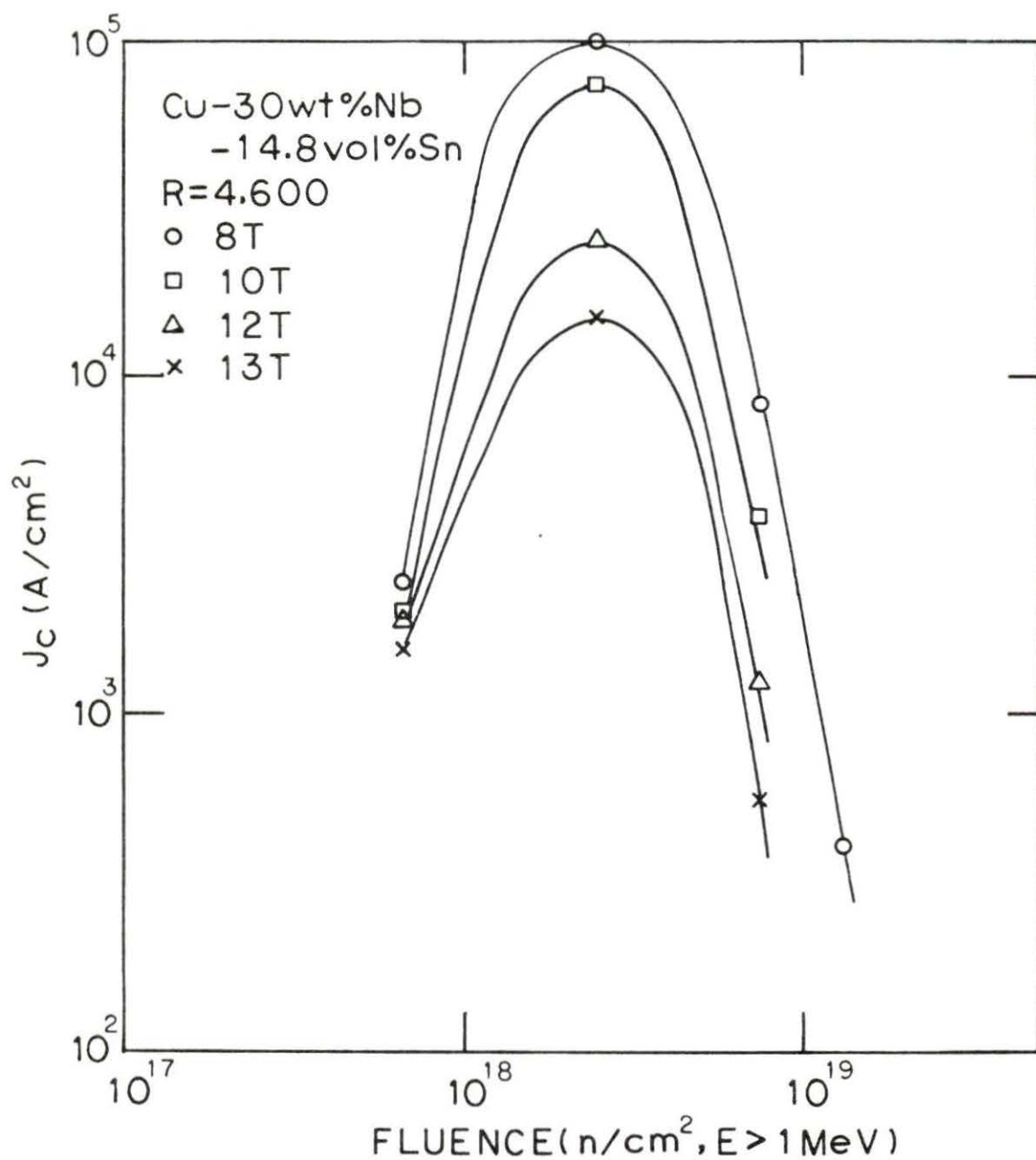


Figure 10. The critical current density of Nb₃Sn-Cu wires (30 wt % Nb, R = 4600) as a function of neutron fluence for several values of applied magnetic field. (Data obtained by Finnemore *et al.*)

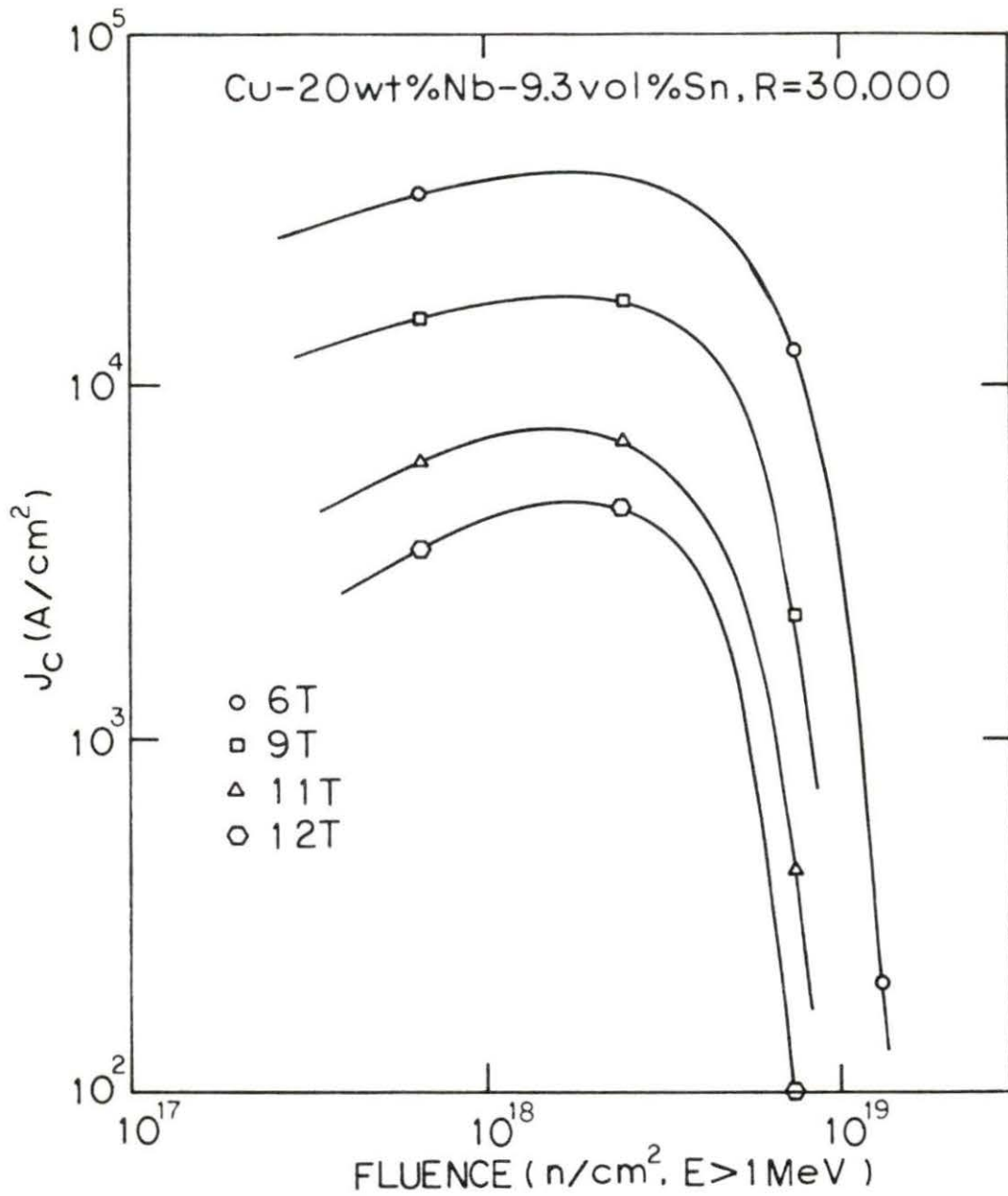


Figure 11. The critical current density of Nb₃Sn-Cu wires (20 wt % Nb, R = 30000) as a function of neutron fluence for several values of applied magnetic field. (Data obtained by Finnemore *et al.*)

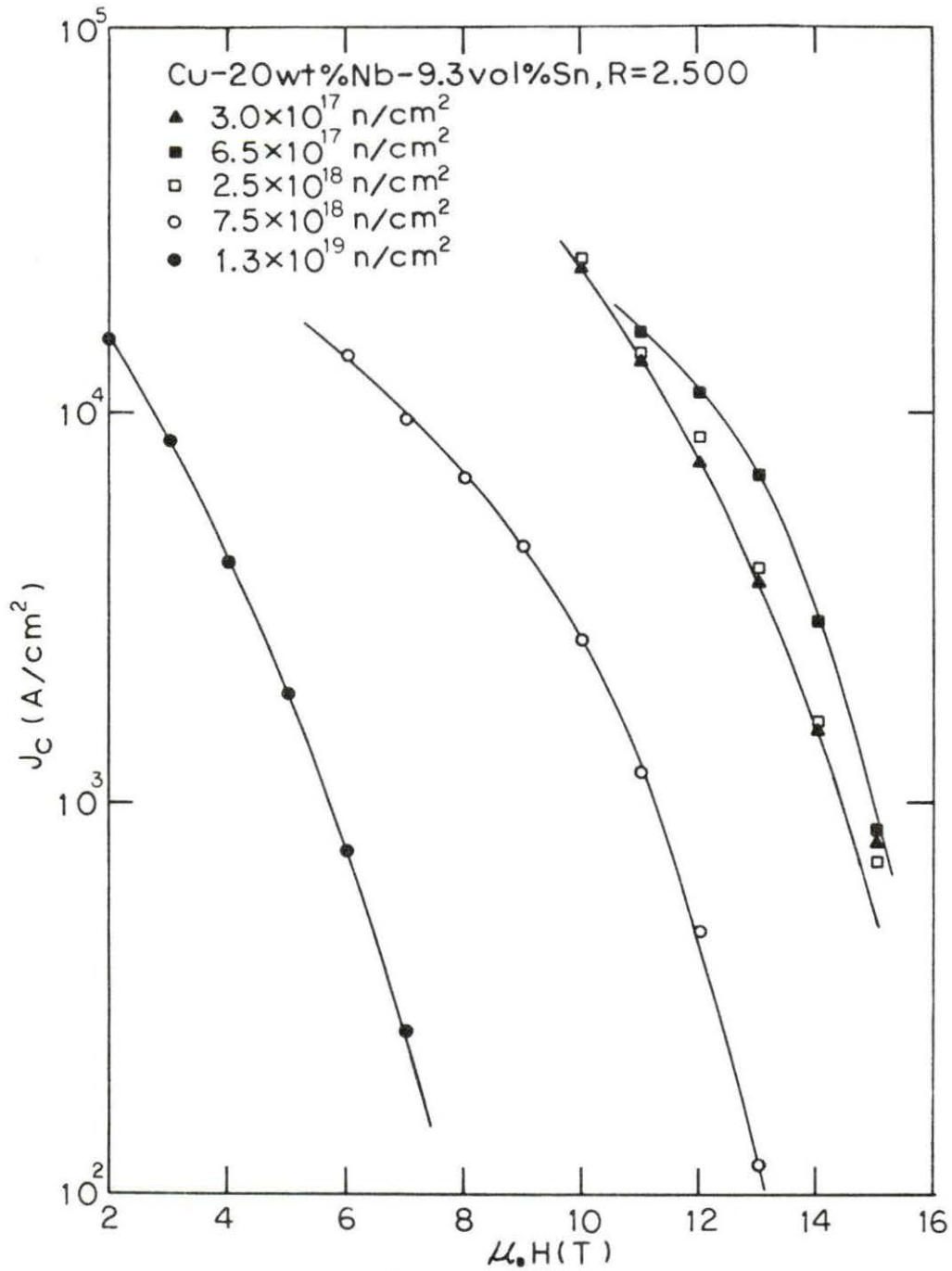


Figure 12. The critical current density of Nb₃Sn-Cu wires (20 wt % Nb, R = 2500) as a function of applied magnetic field for neutron fluence up to 1.3×10^{19} n/cm² ($E > 1$ MeV). (Data obtained by Finnemore *et al.*)

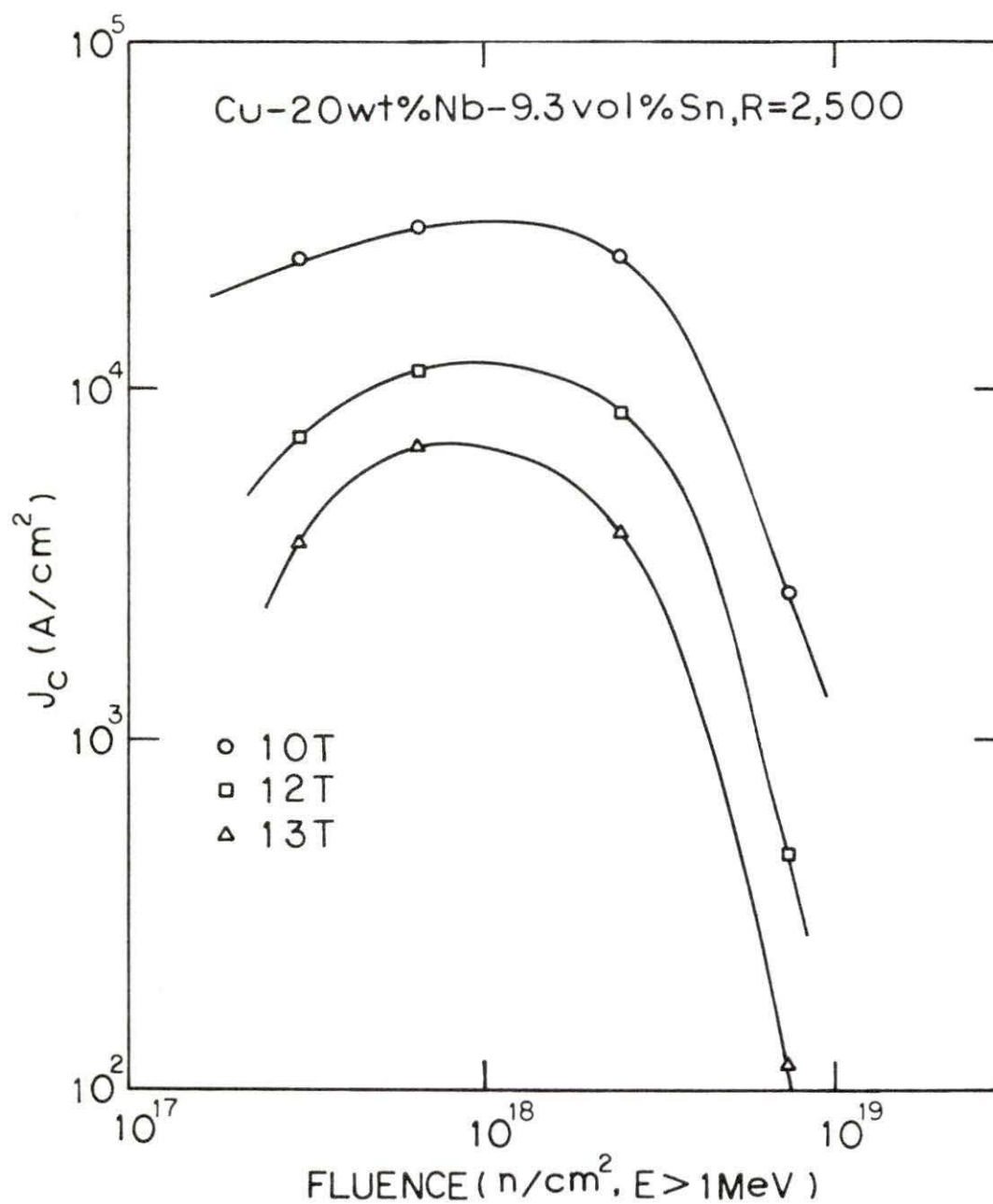


Figure 13. The critical current density of Nb₃Sn-Cu wires (20 wt % Nb, R = 2500) as a function of neutron fluence for several values of applied magnetic field. (Data obtained by Finnemore *et al.*)

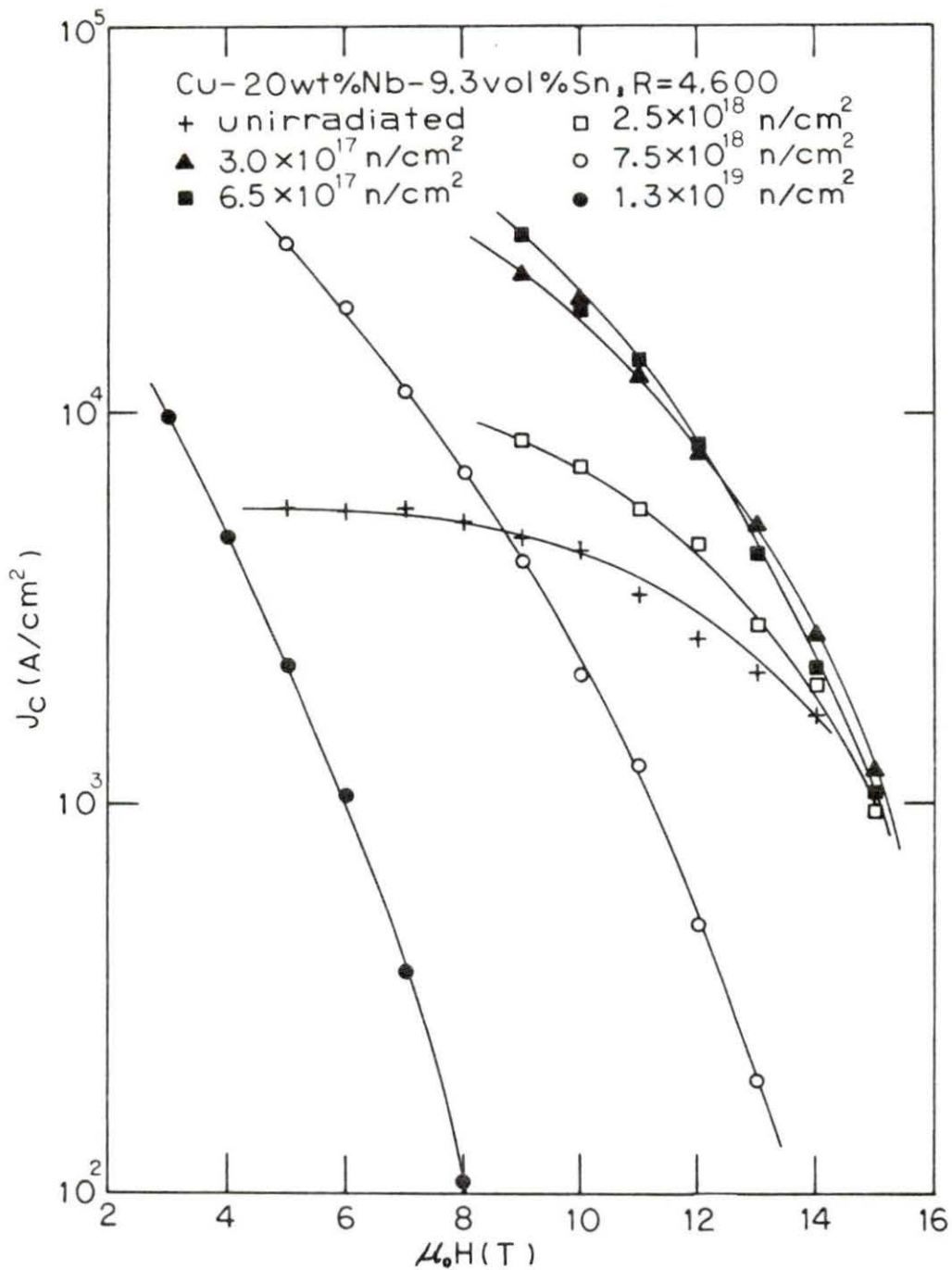


Figure 14. The critical current density of Nb₃Sn-Cu wires (20 wt % Nb, R = 4600) as a function of applied magnetic field for neutron fluence up to $1.3 \times 10^{19} \text{ n/cm}^2$ ($E > 1 \text{ MeV}$). (Data obtained by Finnemore *et al.*)

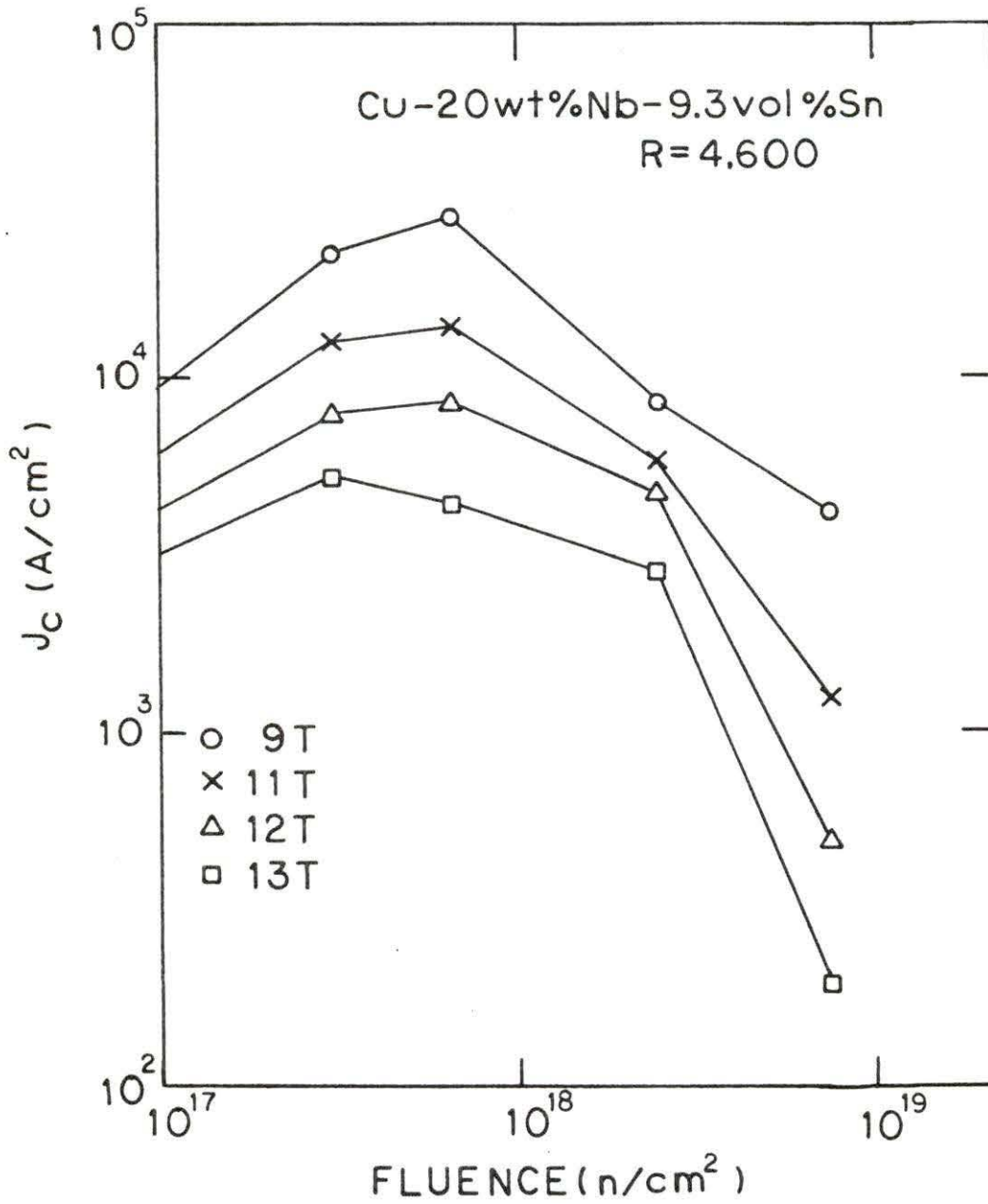


Figure 15. The critical current density of Nb₃Sn-Cu wires (20 wt % Nb, R = 4600) as a function of neutron fluence for several values of applied magnetic field. (Data obtained by Finnemore *et al.*)

critical current density, J_c/J_{c0} , is plotted as a function of neutron fluence for several applied fields in Figure 16. J_{c0} is the critical current density prior to irradiation. It is seen that J_c increases as the fluence increases to 6.5×10^{17} n/cm² for $\mu_0 H \leq 12$ Tesla. The degree of enhancement is clearly greater at lower field values. For higher applied magnetic fields, i.e. $\mu_0 H > 12$ Tesla, J_c increases to a saturation value and then decreases as the fluence increases. The fluence corresponding to saturation is 3.0×10^{17} n/cm². It is also seen that the critical current density is lower than its unirradiated value for $\mu_0 H \geq 9$ Tesla and a fluence of 7.5×10^{18} n/cm².

It will be noted that the significance of Figure 16 is not altered if the values of J_{c0} (the unirradiated values of J_c) shown on Figure 14 are incorrect. The values of J_c/J_{c0} will change, but the break in the curves will occur for the same value of fluence.

The Kramer plots (21) of $J_c^{1/2} B^{1/4}$ versus $\mu_0 H$ are used to determine the upper critical field H_{c2} . The H_{c2} values correspond to the points where linear extrapolations of the $J_c^{1/2} B^{1/4}$ data go to zero. These extrapolated values are given in Table 2.

As seen in Figures 17-20, the data are roughly linear on these plots for the full range of fluence. A theory of flux-lattice shear was proposed by Kramer (21) in accordance with these behaviors. It is supposed that, at high fields, flux motion first occurs when the Lorentz force ($J_c \times B$) on the flux lattice exceeds the lattice shear strength, allowing some portions of the lattice to move relative to more strongly pinned, stationary portions. However, the fact that the Nb₃Sn

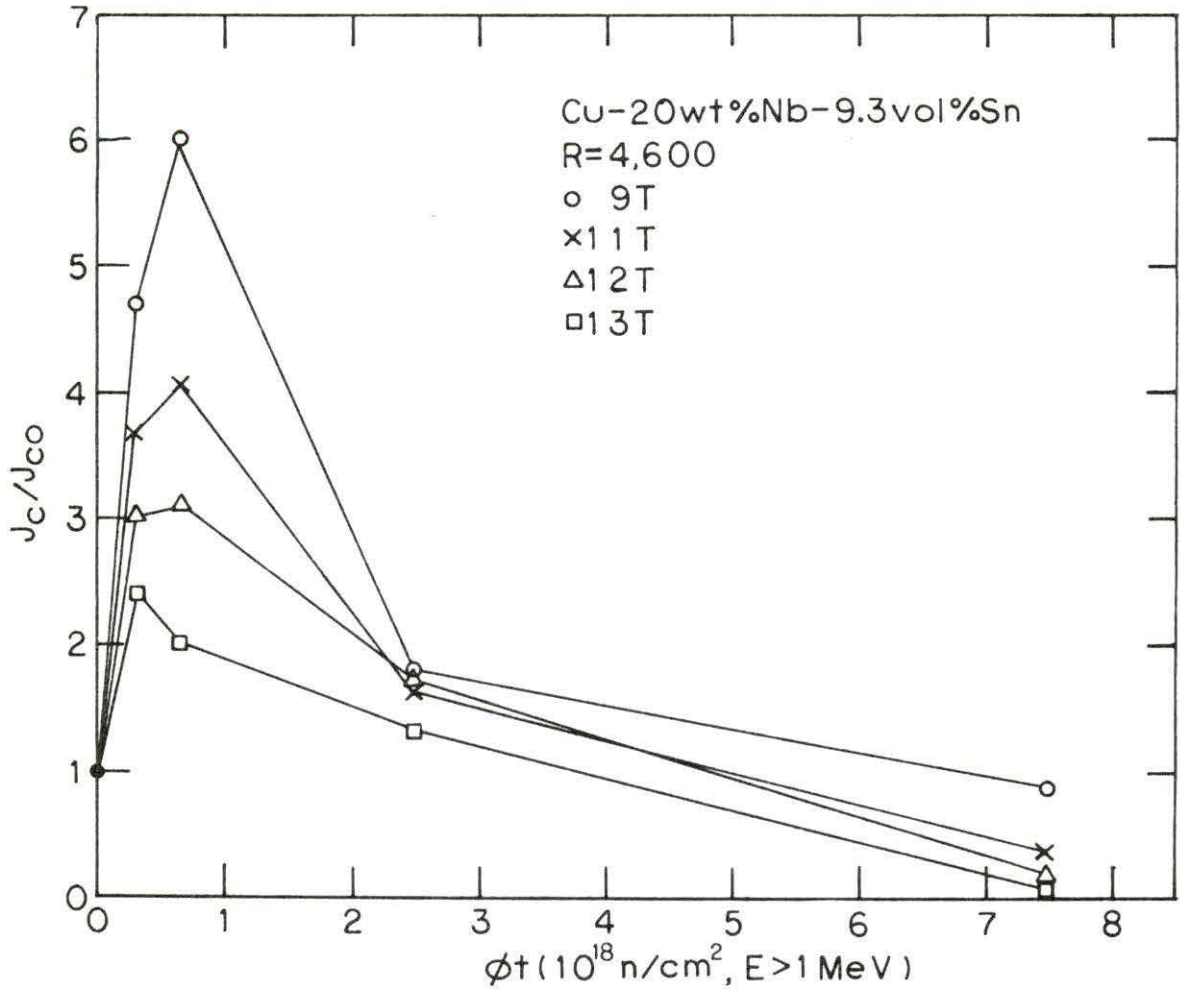


Figure 16. Reduced critical current density J_c/J_{c0} of $\text{Nb}_3\text{Sn-Cu}$ wires (20 wt % Nb, $R = 4600$) plotted as a function of neutron fluence for several applied fields. (J_{c0} is the critical current density prior to irradiation.) (Data obtained by Finnemore *et al.*)

Table 2. Upper critical fields; H_{c2}

Designation	Sample	H_{c2}^a Tesla	H_{c2}^b Tesla	H_{c2}^c Tesla	H_{c2}^d Tesla	H_{c2}^e Tesla
1	Cu-30 wt % Nb - 14.8 vol % Sn R = 4600		-- ^f	16.75	15.12	9
2	Cu-20 wt % Nb - 9.3 vol % Sn R = 2500	15.62	16.12	15.62	13.62	8
3	Cu-20 wt % Nb - 9.3 vol % Sn R = 4600	17.12	16.87	-- ^f	14	8.75
4	Cu-20 wt % Nb - 9.3 vol % Sn R = 30000		15.38	15.75	13	7.12

^a H_{c2} after neutron irradiation at 3.0×10^{17} n/cm².

^b H_{c2} after neutron irradiation at 6.5×10^{17} n/cm².

^c H_{c2} after neutron irradiation at 2.5×10^{18} n/cm².

^d H_{c2} after neutron irradiation at 7.5×10^{18} n/cm².

^e H_{c2} after neutron irradiation at 1.3×10^{19} n/cm².

^fAnomalous data, see Figures 17 and 20.

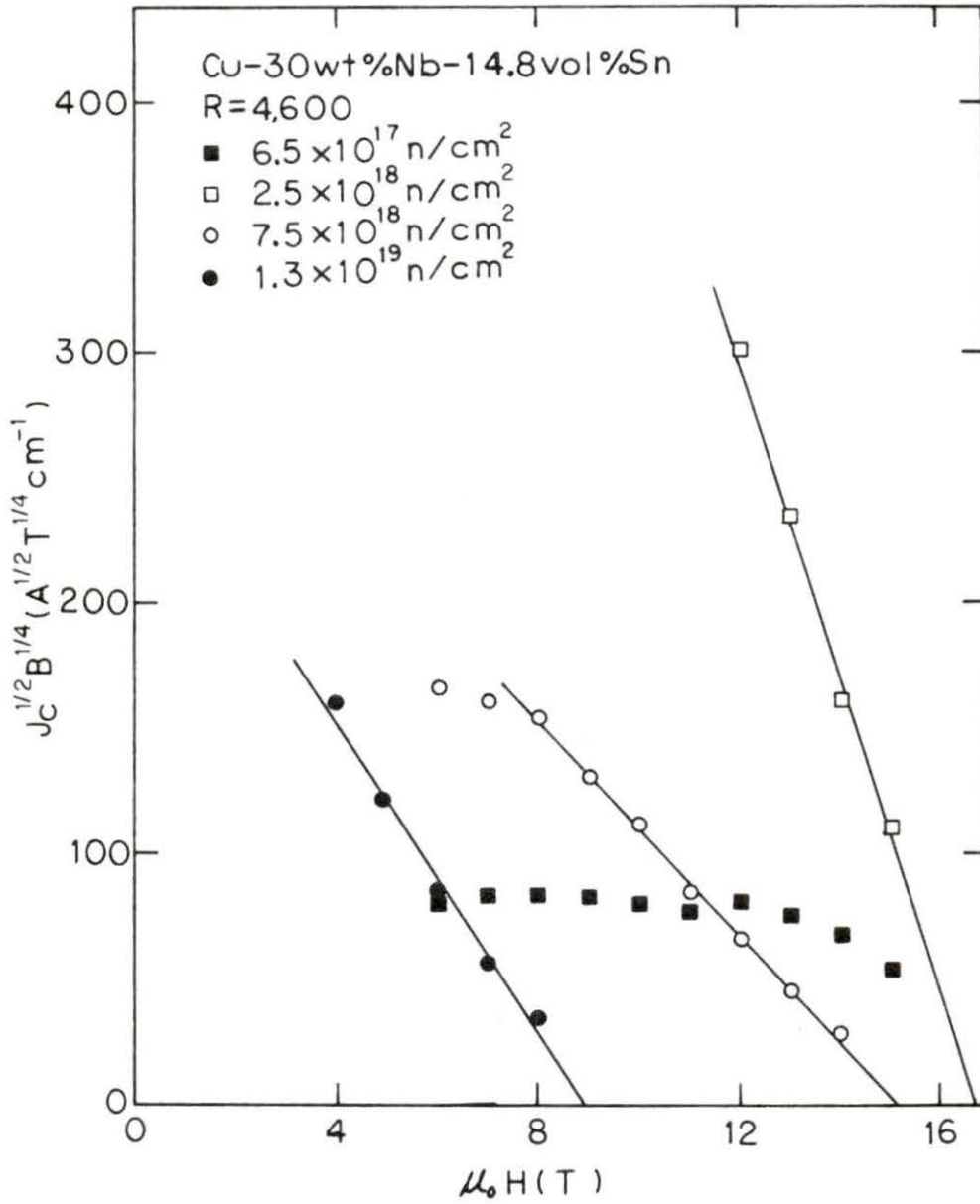


Figure 17. Plot of $J_c^{1/2} B^{1/4}$ versus $\mu_0 H$ for $\text{Nb}_3\text{Sn-Cu}$ wires (30 wt % Nb, $R = 4600$) after irradiation

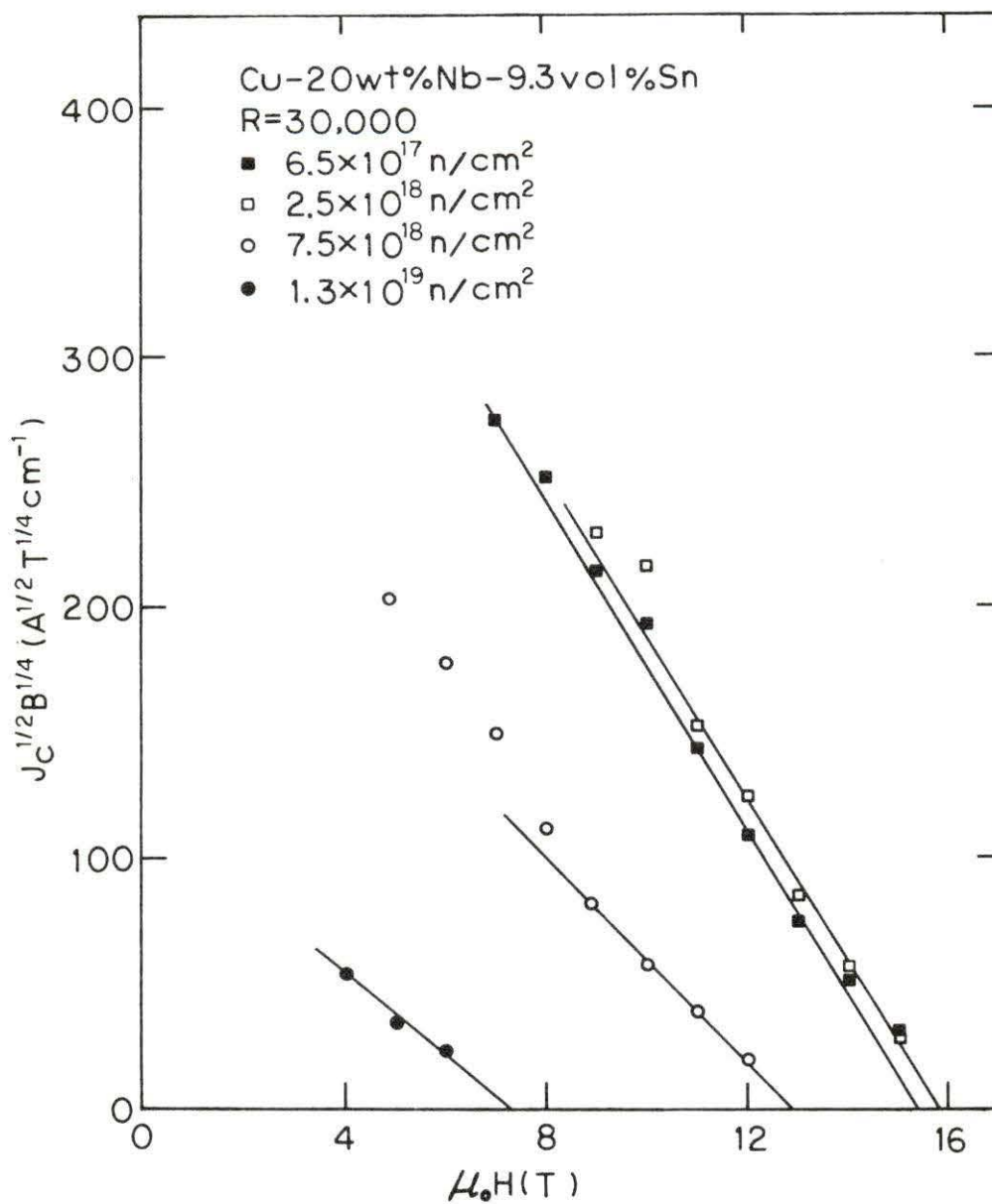


Figure 18. Plot of $J_C^{1/2} B^{1/4}$ versus $\mu_0 H$ for Nb₃Sn-Cu wires (20 wt % Nb, R = 30000) after irradiation

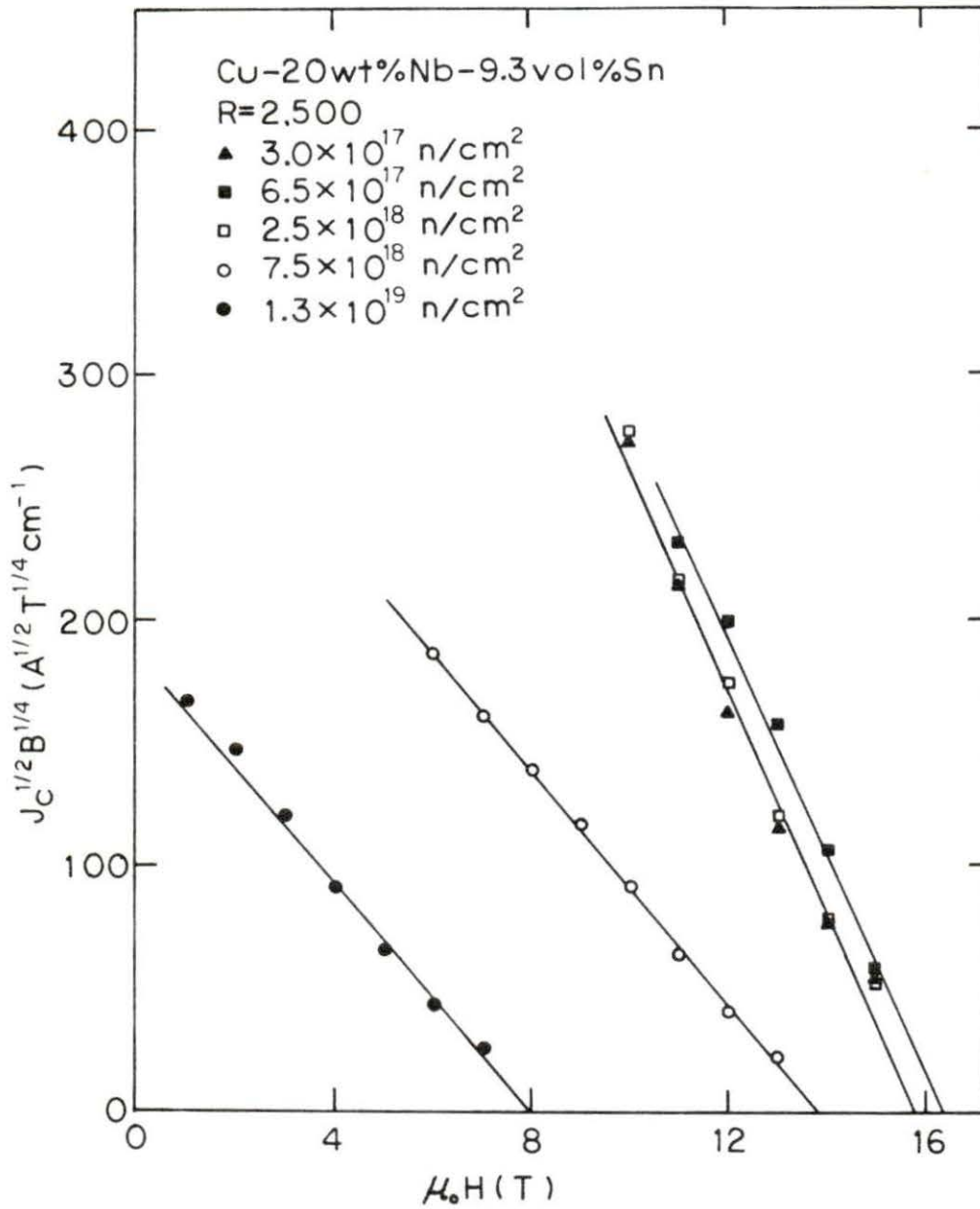


Figure 19. Plot of $J_C^{1/2} B^{1/4}$ versus $\mu_0 H$ for Nb₃Sn-Cu wires (20 wt % Nb, R = 2500) after irradiation

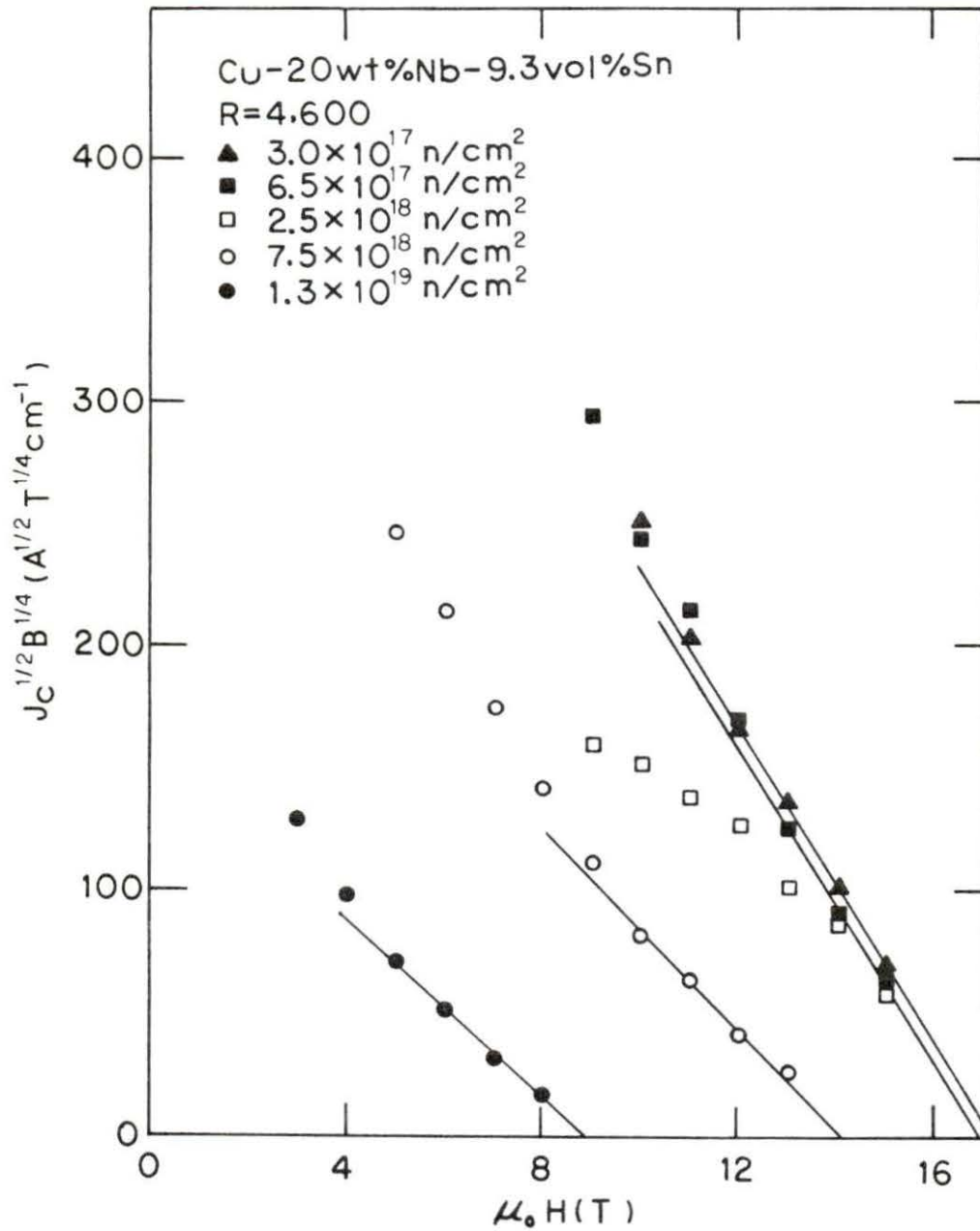


Figure 20. Plot of $J_c^{1/2} B^{1/4}$ versus $\mu_0 H$ for Nb₃Sn-Cu wires (20 wt % Nb, R = 4600) after irradiation

J_c data are linear on the Kramer plots does not mean that shear forces control J_c at high field for in situ wires. The experimental results of Sue et al. (22) indicate that the surface pinning with core interaction rather than flux line shear is applicable for Nb_3Sn in situ wires. The Kramer plots can, nevertheless, still be used to determine H_{c2} since both core pinning on surfaces and flux line shear have the same behavior at high fields. It is seen from Figures 17-20 that the behavior of H_{c2} upon irradiation follows the pattern of J_c as shown in Figures 8, 9, 12, and 14.

V. DISCUSSION

For inhomogeneous and highly anisotropic materials such as these, it is important to point out: a) that the transitions are fairly broad in comparison with those of homogeneous materials, and b) that the value of T_c depends on how it is measured. When the measurements of T_c were made with resistance technique (Figure 5), a measuring current was directed parallel to the long axis of the filaments (and of the wire). Because the filaments of these in situ wires are discontinuous and separated by a Cu layer, the proximity effect may play an important role in the transition temperature. Therefore, ac susceptibility measurements of T_c (Figure 6) were made in which currents are induced around the circumference of the wire perpendicular to the long axis of the filaments. This means that the induced current must cross through the Cu barriers separating the filaments so this susceptibility measures the onset of appreciable proximity coupling. Thus, as can be seen from a comparison of Figures 5 and 6, the value of T_c obtained by the ac susceptibility technique is about 4 K lower than the value obtained by the resistance measurement.

Since in a practical system a liquid helium cryostat operating at a temperature of 4.2 K will be used, the chosen superconducting material will function as desired as long as its value of T_c (degraded by irradiation) is above the limiting temperature of 4.2 K. Thus, from this point of view, the limiting fluence is found by extrapolation (see Figure 5) to be about $3.2 \times 10^{19} \text{ n/cm}^2$.

In broad outline, T_c , J_c , and H_{c2} of the in situ wires show a remarkable decrease with fluence above 10^{18} n/cm². Below this "threshold" fluence, where the depression of T_c is slight, J_c and H_{c2} show enhancements upon irradiation. Since the real microscopic description of radiation-induced defect arrangements is deficient, it is not possible to give basic and clear explanations for the observed behaviors of these irradiated samples. However, the decrease of T_c with increasing fluence can be interpreted by considering the crystallographic structure of the compound (23). Nb_3Sn with an A-15 structure is characterized as having the Nb atoms arranged in a three-dimensional network of orthogonal linear chains. It is well-known that the superconducting properties, especially the transition temperature, are very sensitive to the degree of atomic order (i.e. Nb sites occupied by Nb atoms and Sn sites occupied by Sn atoms). A high T_c is associated with a highly ordered structure. By fast neutron irradiation, some Nb atoms may be replaced by Sn atoms (antisite defects) or vacancies may be introduced in these chains (atomic disordering), leading to a strong reduction of the transition temperature T_c .

In a high magnetic field, the field penetrates the superconductor in the form of a lattice of singly quantized current vortices. When a transport current is applied to the superconductor, a Lorentz force acts on the vortex, or flux line, lattice and in a perfectly homogeneous material, this force would cause the vortex to move and dissipate energy viscously, leading to the appearance of a voltage across the current leads. A practical material is not homogeneous and any inhomogeneity will

act as a pinning site which will tend to "pin" the vortex lattice. Such pinning sites can be second phases, dislocation loops, vacancy and interstitial loops or grain boundaries. For unirradiated Nb_3Sn , it was found (22) that grain boundaries surfaces with core interactions were the only defects present in sufficient density to account for flux pinning. The critical current which can be carried at a particular magnetic field is the current producing the maximum Lorentz force which can be resisted by the pinning sites. At low values of radiation dose (10^{18} n/cm²), the depression of T_c is small. Irradiation introduces defects which are randomly distributed in the Nb_3Sn and act as new pinning sites. The effect of these randomly located radiation-induced defects is added to that of the grain boundaries. In this case, J_c will be influenced by a decrease in electron mean free path due to electron scattering by these pinning sites (24) and a change in the vortex lattice pinning by these pinning sites. Therefore, it is observed that J_c and H_{c2} , initially, increase with increasing fluences.

Thus, irradiation can increase pinning. If, on the other hand, Nb_3Sn wire already contains an appropriate, or saturated, density of pinning sites, either because of its production method or because it has been irradiated, then the introduction of further radiation-induced defects will reduce the effectiveness of the pinning since the defects will begin to overlap. However, this may be only a partial explanation of the reduction of J_c at higher fluences. Part of the reduction in J_c will also be caused by the decrease in the transition temperature, as shown in Figures 21 and 22. For J_c increasing with fluence up to a

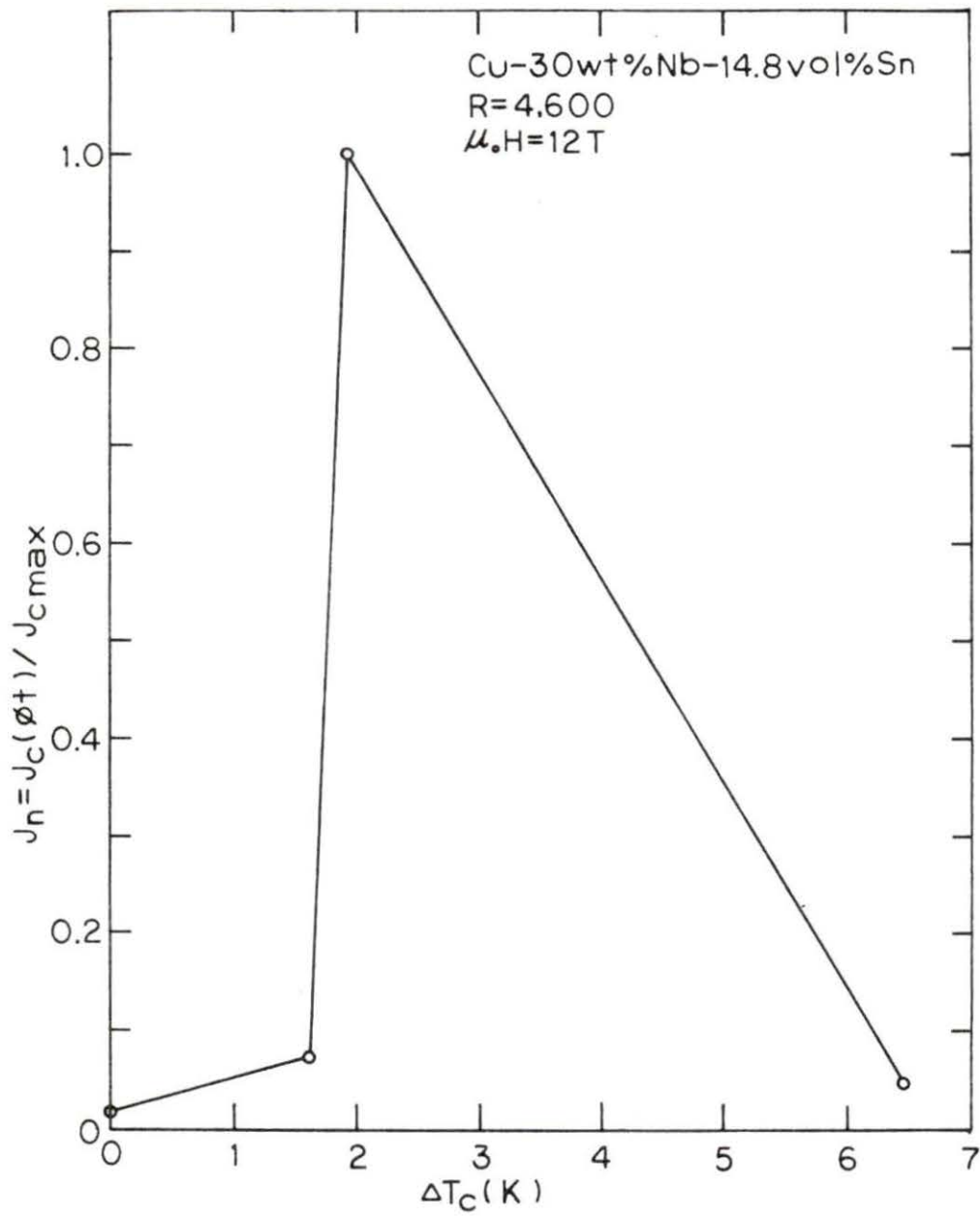


Figure 21. Normalized critical current density as a function of transition temperature reduction ΔT_c for Nb_3Sn -Cu wires (30 wt % Nb, $R = 4600$) upon irradiation. (The solid line is drawn for guiding the eye only)

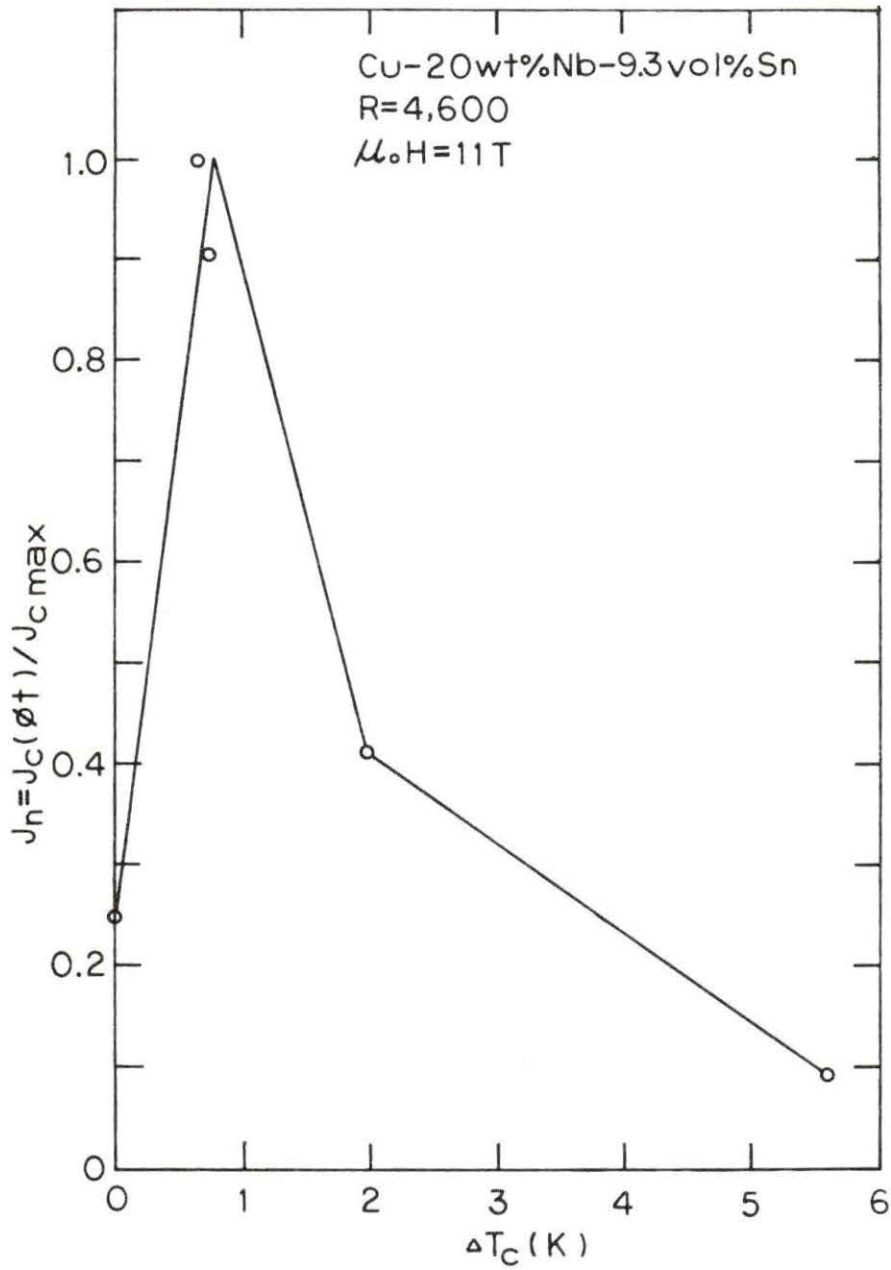


Figure 22. Normalized critical current density as a function of transition temperature reduction ΔT_c for Nb_3Sn -Cu wires (20 wt % Nb, $R = 4600$) upon irradiation. (The solid line is drawn for guiding the eye only)

maximum value J_{cmax} , the reduction of T_c is small at this fluence range. With the rapid drop of T_c , J_c decreases accordingly. Since the upper critical field depends on the transition temperature, the reduction of T_c will also lower H_{c2} , thus causing rapid J_c depressions, as may be seen in Figure 23. The figure indicates that, for 20 wt % Nb - 9.3 vol % Sn ($R = 2500$) wires, H_{c2} and T_c have the same dependence on fluence for values of fluence $> 10^{18}$ n/cm². The same behavior holds for the other in situ wires.

The selection of superconductors for practical applications, such as the magnet coils for fusion reactors, will be based, to a great extent, on the values of J_c , H_{c2} , and T_c and on how these parameters change with neutron irradiation. Other considerations being equal, high values of all three are desired, both initially and after an irradiation period. Figure 24 shows how J_c measured, at 14 Tesla, varies with fluence for the four groups of in situ wires. Based on the values of J_c , 30 wt % Nb - 14.8 vol % Sn ($R = 4600$) wires have a better fluence tolerance than do the wires with different compositions. Thus, this material with the reduction ratio of 4600 provides the best superconducting properties for the materials tested. Although the J_c of 20 wt % Nb - 9.3 vol % Sn ($R = 2500$) wires and 20 wt % Nb - 9.3 vol % Sn ($R = 4600$) wires decrease for fluences higher than 6.5×10^{17} n/cm² and 3.0×10^{17} n/cm², respectively, the values of J_c are still higher than that obtained with a 20 wt % Nb - 9.3 vol % Sn ($R = 30000$) wire at a fluence of 2.5×10^{18} n/cm², where the J_c of the 20 wt % Nb - 9.3 vol % Sn ($R = 30000$) wire shows enhancement. Severe reduction of

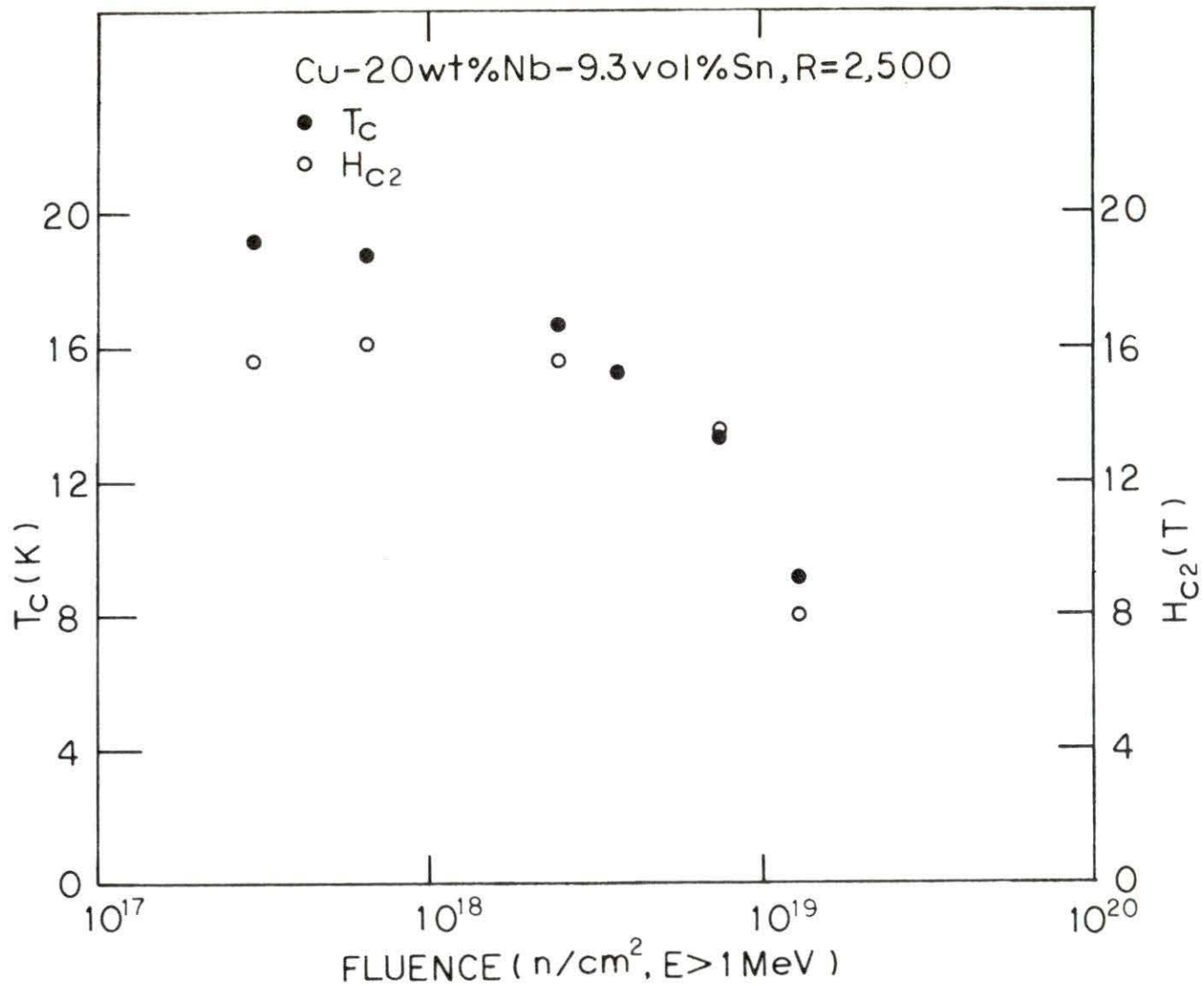


Figure 23. Comparison of H_{c2} and T_c for Nb_3Sn -Cu wires (20 wt % Nb, R = 2500)

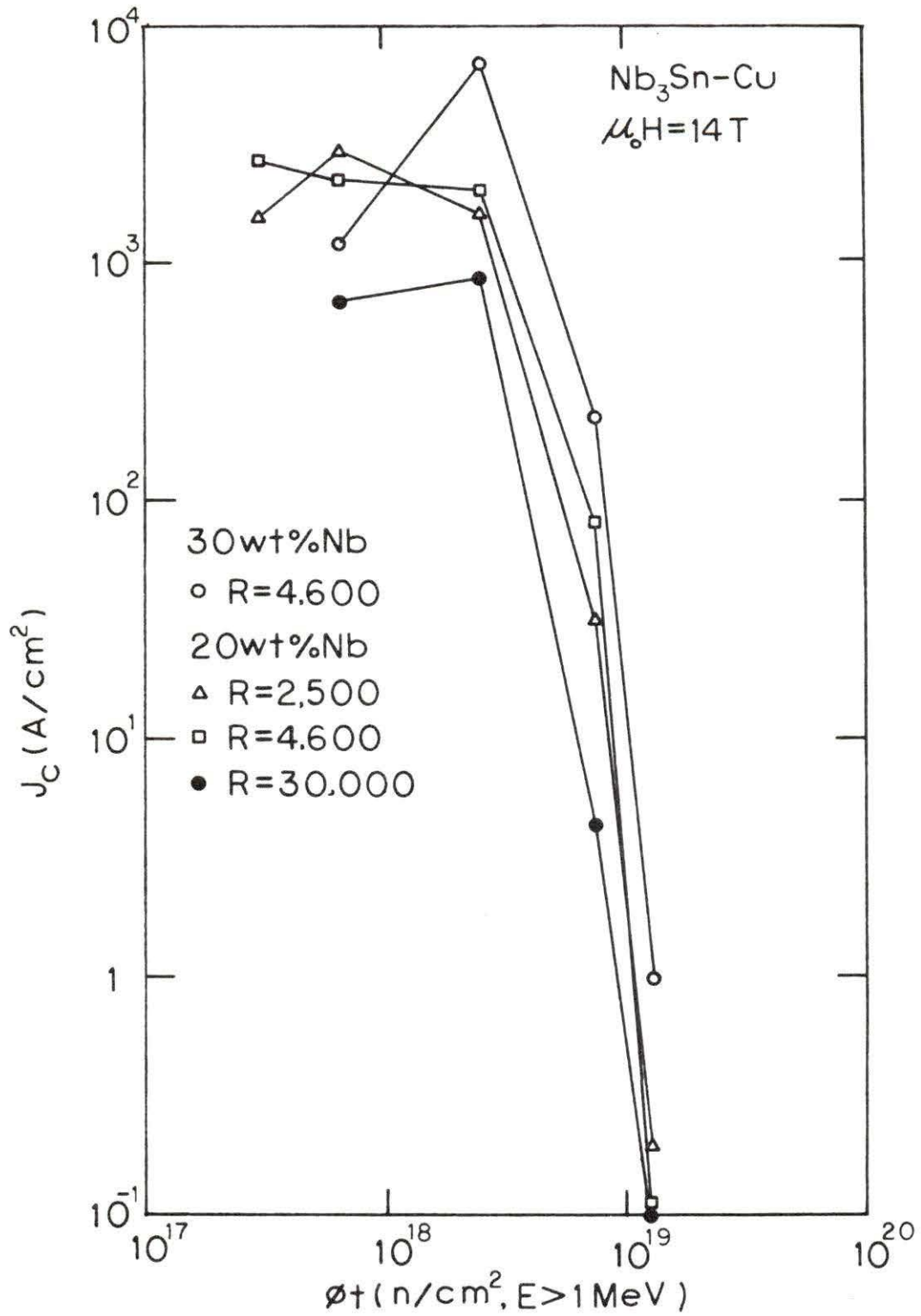


Figure 24. Critical current density of a family of $\text{Nb}_3\text{Sn-Cu}$ in situ wires versus neutron fluence at 14 Tesla

J_c was observed for all wires at a fluence of 1.3×10^{19} n/cm².

As mentioned in the Introduction, the lifetime dose for material in the magnet region is estimated to be $\sim 2.0 \times 10^{18}$ n/cm² for a ten-year life operation. Thus, on the basis of the measurement reported, Nb₃Sn-Cu superconducting composite with higher Nb content appears to be an excellent candidate material for magnets to be used to confine the plasma in fusion reactors.

An attempt has been made to calculate H_{c2} (4.2 K) and J_c values under the assumption that T_c is the only variable changed by the irradiation (model-1). This clearly is a major effect and an attempt is made here to ascertain how much of the changes in J_c come from this variable. If we assume that the mean free path in the superconductor and the density of electronic states do not change,

$$H_{c2}(T) = H_{c2}(0) \left(1 - \frac{T^2}{T_c^2}\right), \quad (1)$$

and

$$H_{c2}(0) = 3 \times 10^4 \gamma_N T_c, \quad (2)$$

then a law of corresponding states should hold and the critical field curves should be similar. As was shown earlier (25),

$$J_c = A H^{-1/2} (H_{c2} - H)^2 \quad (3)$$

describe these data rather well. If the sample irradiated to a neutron fluence of 2.5×10^{18} n/cm² is used as a reference to infer the values

of $H_{c2}(0)$ and A , then one can derive the J_c results for samples with higher irradiated doses. The results of these calculations are shown as broken lines in Figures 25a and 25b. The solid lines represent a guide to the eye for the experimental results. If we assume that the specific heat (γ) and the normal state resistivity (ρ_N) of superconductor do not change upon irradiation, the upper critical field at absolute zero $H_{c2}(0)$ can be represented as $H_{c2}(0) = 3 \times 10^4 \gamma \rho_N T_c$ (26). From Equation (1), the $H_{c2}(0)$ value for the reference sample can be inferred first by fitting the data. Then, Equation (4),

$$\frac{H_{c2}(0)}{H_{c2}(0)_{\text{Ref.}}} = \frac{T_c}{T_{c \text{ Ref.}}} \quad (4)$$

is used to calculate the $H_{c2}(0)$ values for samples with higher irradiated doses. Again, by substituting the $H_{c2}(0)$ values into Equation (1), the H_{c2} values at 4.2 K for samples with higher irradiated doses can be obtained. It is assumed here that T_c is the measured value shown on Figure 5.

J_c values at different applied magnetic fields H can be obtained by substituting the $H_{c2}(4.2 \text{ K})$ values into Equation 3. The constant A , the square of the slope of the reference line in Figure 25b, is $3844 \text{ A cm}^{-2} \text{ T}^{-3/2}$.

As can be seen from Figures 25a and 25b, the calculated data (dashed and dot-dash lines), based on the assumptions that γ and ρ_N are constant upon irradiation, have higher $A^{1/2}$ values (slopes) than that of the experimental data (solid lines). The experimental data have

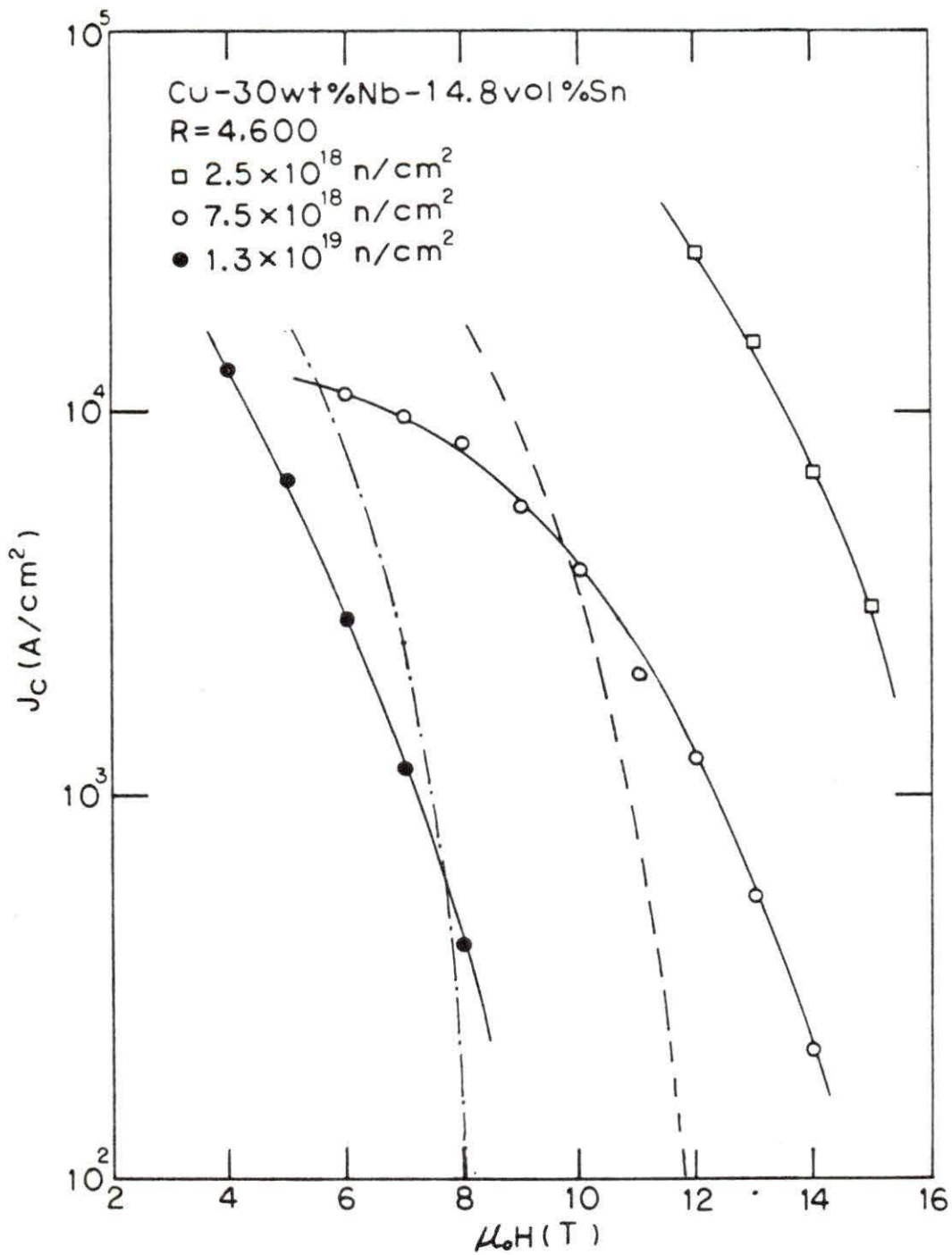


Figure 25a. The critical current density as a function of applied magnetic field for neutron fluence up to 1.3×10^{19} n/cm² ($E > 1$ MeV). The dashed line and the dot-dash line, model-1 calculations which assume that T_c is the only variable changed upon irradiation, are for 7.5×10^{18} n/cm² and 1.3×10^{19} n/cm², respectively

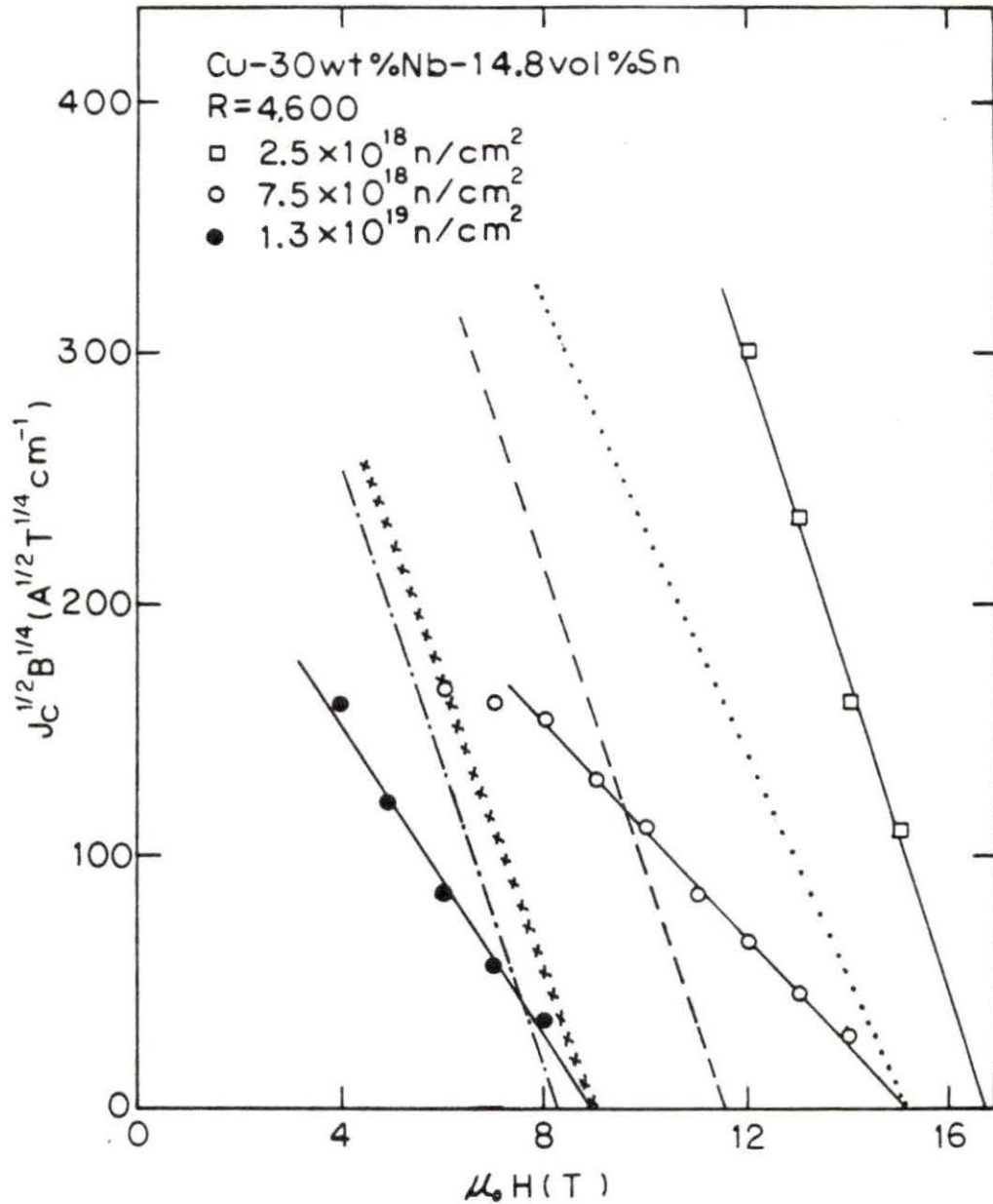


Figure 25b. Comparison of the data with model-1 calculations which assume that T_c is the only variable changed, and with model-2 calculations which assume that T_c and ρ_N are the only variables changed upon irradiation. Dashed line (model-1) and dotted line (model-2) are for 7.5×10^{18} n/cm². Dot-dash line (model-1) and crossed line (model 2) are for 1.3×10^{19} n/cm².

lower $A^{\frac{1}{2}}$ values (slopes) indicating higher values of Ginzburg-Landau constant κ . As we know $\kappa = 7.5 \times 10^3 \gamma^{\frac{1}{2}} \rho_N$, therefore, the experimental data are consistent with a higher normal state resistivity ρ_N than was used in obtaining the calculated data. Thus, a conclusion can be drawn that the normal state resistivity ρ_N will be increased upon irradiation.

Since $H_{c2} = \kappa \sqrt{2} H_c$, the higher κ values also indicate higher H_{c2} values.

Another attempt was made to obtain the calculated data under the assumption that T_c and ρ_N are the variables changed by the irradiation (model-2). Since $H_{c2} = \kappa \sqrt{2} H_c$, we can deduce the equation

$$\frac{\kappa_{\text{model-2}}}{\kappa_{\text{model-1}}} = \frac{H_{c2 \text{ model-2}}}{H_{c2 \text{ model-1}}} \quad . \quad (5)$$

By substituting values of $H_{c2 \text{ model-2}}$ and $H_{c2 \text{ model-1}}$, we can obtain the ratio of $\kappa_{\text{model-2}}/\kappa_{\text{model-1}}$ which corresponds to the ratio of $(A_{\text{model-1}}/A_{\text{model-2}})^{\frac{1}{2}}$. The slope, $A^{\frac{1}{2}}$ value, of the calculated data (model-2) can, therefore, be obtained. These data are shown in Figure 25b as a dotted line for $7.5 \times 10^{18} \text{ n/cm}^2$ and as a crossed line for $1.3 \times 10^{19} \text{ n/cm}^2$. The fact that the experimental data (solid lines) have lower $A^{\frac{1}{2}}$ values than those of the calculated data (model-2) indicates that irradiation influences the pinning mechanisms in addition to its effects on T_c and ρ_N .

VI. SUMMARY AND CONCLUSIONS

A-15 superconducting compounds, in situ Nb₃Sn-Cu wires, were irradiated at 80°C and the changes of superconducting properties induced by irradiation were investigated.

The following conclusions are drawn:

1. An apparent threshold fluence of $\sim 10^{18}$ n/cm² (E > 1 MeV) is required to bring about severe depressions in T_c. Below this value, no significant deterioration in T_c is observed.
2. In general, Nb₃Sn-Cu wires show a catastrophic reduction in J_c above a fluence of $\sim 2 \times 10^{18}$ n/cm². J_c increases with dose at lower fluence for all the wires studied.
3. H_{c2} values follow the pattern of J_c upon irradiation.
4. An explanation of the effect of neutron irradiation is thought to be first, disordering, causing a lowering of T_c; and second, radiation-induced inhomogeneities occur initially enhancing and then reducing vortex pinning.
5. The effect of the radiation on the superconducting magnet used for a CTR (Controlled Thermonuclear Reactor) device will not present a serious deterioration of superconducting properties provided the fluence does not exceed $\sim 2 \times 10^{18}$ n/cm² (E > 1 MeV). If the wires investigated in this work are exposed to higher fluences, a severe degradation takes place both in T_c and J_c making these materials unsuitable for further service as magnet

conductors. If longer service, producing higher fluences, is required, then appropriate shielding must be provided to prevent the dose received by the superconducting wires below the experimentally determined limit of about $\sim 2 \times 10^{18} \text{ n/cm}^2$ ($E > 1 \text{ MeV}$).

VII. SUGGESTIONS FOR FURTHER STUDY

The results of the studies reported in this thesis indicate that of the four in situ samples tested, the one identified by the 30 wt % Nb - 14.8 vol % Sn (R = 4600) is the most suitable candidate for a fusion reactor magnet coil. The investigations have raised certain questions which are presented as topics for further study.

1. What effect does neutron irradiation carried out at low temperature (i.e. 10 K) have on the superconducting properties of in situ prepared wires? (Recall that the irradiations discussed in this thesis were carried out at about 80°C.)
2. Can the lifetime of the superconducting material be extended by annealing? If so, at what fluence should the anneal be performed? What temperature would be most appropriate? What would be the most suitable duration for the anneal? How are the factors (a) achieved fluence before anneal, (b) temperature of the anneal, and (c) duration of the anneal related? Would other wires be a better choice if annealing is to be considered?

VIII. REFERENCES

1. G. M. McCracken and S. Blow, Culham Laboratory Report, CLM-R120 (1972).
2. J. J. Sue, J. D. Verhoeven, E. D. Gibson, J. E. Ostenson and D. K. Finnemore, *Acta Met.* 29, 1791 (1981).
- 3a. M. Suenaga, W. B. Sampson and T. S. Luhman, *IEEE Trans. Magn.* MAG-17, 646 (1981).
- 3b. J. E. Ostenson, D. K. Finnemore, J. D. Verhoeven, E. D. Gibson and C. L. Snead, Jr., *IEEE Trans. Magn.* MAG-19, 777 (1983).
4. P. S. Swartz, H. R. Hart and R. L. Fleischer, *Appl. Phys. Lett.* 4, 71 (1964).
5. J. L. Cooper, *RCA Rev.* 25, 405 (1964).
6. R. Bett, *Cryogenics* 14, 361 (1974).
7. A. R. Sweedler, D. G. Schweitzer and G. W. Webb, *Phys. Rev. Lett.* 33, 168 (1974).
8. H. Bauer, E. J. Saur and D. G. Schweitzer, *J. Low Temp. Phys.* 19, 171 (1975).
9. M. Soell, H. Bauer, K. Boening and R. Bett, *Phys. Lett.* 51A, 83 (1975).
10. M. Soell, K. Boening and H. Bauer, *J. Low Temp. Phys.* 24, 631 (1976).
11. G. W. Cullen and L. Novak, *Appl. Phys. Lett.* 4, 147 (1964).
12. G. W. Cullen, R. L. Novak and J. P. McEvoy, *RCA Rev.* 25, 479 (1964).
13. G. W. Cullen and R. L. Novak, *J. Appl. Phys.* 37, 3348 (1967).
14. D. M. Parkin and D. G. Schweitzer, *Nucl. Technol.* 22, 108 (1974).
15. B. S. Brown, T. H. Blewitt, D. G. Wozniak and M. Suenaga, *J. Appl. Phys.* 46, 5163 (1975).
16. D. M. Parkin and A. R. Sweedler, *IEEE Trans. Magn.* MAG-11, 166 (1975).
17. C. L. Snead, Jr., *Appl. Phys. Lett.* 30, 662 (1977).
- 18a. R. R. Hake, *Phys. Rev.* 158, 356 (1967).

- 18b. D. K. Finnemore. Private Communication, Ames Laboratory, DOE, Ames, Iowa (1984).
19. C. L. Snead, Jr., D. M. Parkin and M. W. Guinan, *J. Nuc. Mat.* 103, 749 (1981).
20. A. R. Sweedler, D. E. Cox and S. Moehlecke, *J. Nuc. Mat.* 72, 50 (1978).
21. E. J. Kramer, *J. Appl. Phys.* 44, 1360 (1973).
22. J. J. Sue, D. K. Finnemore, J. E. Ostenson, E. D. Gibson and J. D. Verhoeven, in *Advances in Cryogenic Engineering Materials*, edited by R. P. Reed and A. F. Clark (Plenum Press, New York, 1982), Vol. 28, p. 323.
23. M. Soell, *J. Nuc. Mat.* 72, 122 (1978).
24. W. E. Yetter, D. A. Thomas and E. J. Kramer, *Philos. Mag. B*, 46, 523 (1982).
25. D. K. Finnemore, J. E. Ostenson, E. D. Gibson, J. D. Verhoeven and T. B. Doyle, *J. Appl. Phys.* 54, 1476 (1983).
26. P. G. de Gennes, Superconductivity of Metals and Alloys (W. A. Benjamin, Inc., New York, 1966).

IX. ACKNOWLEDGMENTS

I would like to express my sincere gratitude to Dr. Donald M. Roberts, my thesis advisor, for all of his patient guidance, continuous encouragement and invaluable instruction.

I extend appreciation to Dr. D. K. Finnemore for his patience and assistance during the course of this study and for serving as a member of my graduate committee. I especially appreciate him for providing the all critical current data. Also, I am grateful to Dr. R. A. Danofsky for serving as a member of my graduate committee.

I am grateful to Associate Physicist J. E. Ostenson of the Physics Department for assistance in T_c measurements, and for valuable discussion. Part of this study (J_c measurements) was performed while Dr. D. K. Finnemore and Associate Physicist J. E. Ostenson were guest scientists at the Francis Bitter National Magnet Laboratory which is supported at M.I.T. by the National Science Foundation.